GATA6 regulates WNT and BMP programs to pattern precardiac mesoderm during the earliest stages of human cardiogenesis

Joseph A. Bisson[1], Miriam Gordillo[1], Ritu Kumar[1,2], Neranjan de Silva[1], Ellen Yang[1], Kelly M. Banks[1], Zhong-Dong Shi[3], Kihyun Lee[3,4], Dapeng Yang[3], Wendy K. Chung[5], Danwei Huangfu[3], and Todd Evans[1,6,7,*]

[1] Department of Surgery, Weill Cornell Medicine, New York, NY, 10065, USA
[2] current address: Gladstone Institutes, San Francisco, CA, 94158, USA
[3] Developmental Biology Program, Sloan Kettering Institute, New York, NY, 10065, USA
[4] current address: College of Pharmacy, Ewha Womans University, Seoul 03760, Republic of Korea
[5] Childrens Hospital, Harvard Medical School, Boston, MA, 02115, USA
[6] Hartman Institute for Therapeutic Organ Regeneration, Weill Cornell Medicine, New York, NY 10065, USA
[7] Center for Genomic Health, Weill Cornell Medicine, New York, NY 10065, USA

Running Title: Gata6 patterns precardiac mesoderm

*Corresponding author: Todd Evans, tre2003@med.cornell.edu

Key words: heart development, congenital heart disease, cardiac progenitors, eomesodermin

Abstract

Haploinsufficiency for *GATA6* is associated with congenital heart disease (CHD) with variable comorbidity of pancreatic or diaphragm defects, although the etiology of disease is not well understood. Here, we used cardiac directed differentiation from human embryonic stem cells (hESCs) as a platform to study GATA6 function during early cardiogenesis. GATA6 loss-of-function hESCs had a profound impairment in cardiac progenitor cell (CPC) specification and cardiomyocyte (CM) generation due to early defects during the mesendoderm and lateral mesoderm patterning stages. Profiling by RNA-seq and CUT&RUN identified genes of the WNT and BMP programs regulated by GATA6 during early mesoderm patterning. Furthermore, interactome analysis detected GATA6 binding with developmental transcription factors and chromatin remodelers suggesting cooperative regulation of cardiac lineage gene accessibility. We show that modulating WNT and BMP inputs during the first 48 hours of cardiac differentiation is sufficient to partially rescue CPC and CM defects in *GATA6* heterozygous and homozygous mutant hESCs. This study provides evidence of the regulatory functions for GATA6 directing human precardiac mesoderm patterning during the earliest stages of cardiogenesis to further our understanding of haploinsufficiency causing CHD and the co-occurrence of cardiac and other organ defects caused by human *GATA6* mutations.

Introduction

Congenital heart disease (CHD) is the most common human birth defect, affecting nearly 1% of live births[1]. CHD is generally understood to derive from dysfunction in the growth, morphogenesis, and/or differentiation of cardiac-fated progenitor cell derivatives; however, the genetic and molecular networks governing these processes remain under investigation. Treatment options are limited to surgical interventions that can save the life of the infant but do not correct the underlying genetics. The causative genetic variants may contribute to complications and morbidity in adulthood[2]. Research aimed to expand our understanding of the molecular genetics regulating normal human cardiogenesis is thus needed to advance therapeutic strategies in the detection and treatment of CHD.

Studies of cardiac development in model organisms have led to the discovery of key molecular drivers of heart organogenesis, including the GATA family of zinc-finger transcription factors. GATA factors, named by their ability to bind to the consensus sequence (*A*/*T*)*GATA*(*A*/*G*)[3], represent six family members with GATA4/5/6 expressed in the developing heart of early stage embryos[4,5]. GATA4/5/6 transcription factors regulate multiple stages of heart development including the specification, proliferation, and differentiation of cardiac progenitor cells (CPCs)[6]. Notably, *GATA6* knockout (KO) mice exhibit early embryonic arrest during primitive streak formation due to defects in visceral endoderm, a phenotype that has complicated the study of the early developmental function of GATA6 *in vivo*[7]. Mice with conditional deletion of *GATA6* from early CPCs develop heart abnormalities including atrioventricular canal defects, ventricular septal defects, and partial loss of trabeculae[8,9]. While these *GATA6* conditional homozygous KO mice die at birth due to heart malformations, few cardiac phenotypes were reported in the *GATA6* heterozygous mutants, except for recent reports of bicuspid aortic valve and heart rhythm abnormalities[10,11].

In humans, heterozygous mutations in *GATA6* are associated with various forms of CHD including outflow tract (OFT) defects, septal defects, and Tetralogy of Fallot[12,13]. GATA6 is required for the development of multiple mesoderm and endoderm derived organs and some CHD patients with heterozygous *GATA6* mutations have comorbidities including pancreatic agenesis, neonatal diabetes, or congenital diaphragmatic hernia[14,15]. The phenotypic diversity of birth defects in patients containing *GATA6* mutations illustrates the complexity of human haploinsufficiency; there is likely a combination of variants in modifying or interacting genes

that converge to influence the disease phenotype[16,17]. Previous studies of the function of *GATA6* in model organisms have not sufficiently modeled the variety of cardiac (and non-cardiac) defects observed in humans and most describe phenotypes only after homozygous inactivation of the gene. This raises an important question; why do CHDs in humans associate with *GATA6* haploinsufficiency? Species-specific functions for GATA6 may differ between mouse and humans, for example, raising the question of how observations made in model organisms relate to human cardiac development. There is a clear need to investigate the function of GATA6 in the context of a human system to better understand the basis for haploinsufficiency.

Current *in vitro* cardiac-directed differentiation protocols for human pluripotent stem cells (hPSCs) provide powerful tools for studying the transcriptional regulatory networks relevant to CHD[18]. A previous study using human induced pluripotent stem cells (hiPSCs) with CRISPR-Cas9 induced *GATA6* mutations showed that GATA6 is required at the stages of CPC and cardiomyocyte (CM) differentiation[19]. GATA6 is also required for definitive endoderm (DE) differentiation toward the pancreatic lineage as reported in several studies using hPSCs[20-23]. However, the function of GATA6 during early mesoderm patterning of human cardiac differentiation has not been explored, and how *in vitro* cardiac and DE lineage phenotypes caused by GATA6 loss-of-function relate to one another is not understood.

To determine the function of GATA6 during the earliest stages of cardiac differentiation, we performed *in vitro* CM directed differentiation using *GATA6* loss-of-function human embryonic stem cell (hESC) lines and explored regulatory functions for GATA6 during precardiac mesoderm patterning that is ultimately required for CM generation. Transcriptome analysis revealed that *GATA6* mutations impaired expression of genes important for lateral and cardiac mesoderm patterning, and by integrating GATA6 CUT&RUN sequencing with RNA-seq we identified GATA6-regulated targets including those of the WNT and BMP networks, key morphogenetic signaling pathways required to induce anterior primitive streak formation[24,25]. Furthermore, we found that GATA6 interacts with important developmental transcription factors and chromatin remodelers during early mesoderm patterning stages that may promote DNA accessibility required for cardiac lineage commitment. Taken together, these findings uncover multiple functions for GATA6 in regulating very early precardiac mesoderm patterning and the lineage specific gene networks required for human CM generation.

Results

GATA6 loss-of-function impairs CM differentiation

A monolayer cytokine-based *in vitro* cardiac differentiation protocol for hPSCs was adapted from previously established methods[26,27] (Figure 1A). *GATA6* heterozygous mutant (*GATA6*$^{+/-}$), homozygous mutant (*GATA6*$^{-/-}$), and isogenic wildtype (WT) control (*GATA6*$^{+/+}$) H1-hESC lines were previously generated[20,28] (Supplemental Figure 1A, B). These lines were differentiated in parallel to determine the impact of *GATA6* loss-of-function during human cardiogenesis. Western blotting at days 2 or 5 of cardiac differentiation confirmed the loss of GATA6 protein in *GATA6*$^{-/-}$ cells and intermediate levels of protein in *GATA6*$^{+/-}$ cells relative to WT controls (Supplemental Figure 1C). The percentage of cardiac troponin T positive (%cTnT^{+}) CMs in individual differentiation assays remained stable starting around day 13 and thus CM differentiation efficiency was analyzed during a window of days 13 to 18 of cardiac differentiation. *GATA6*$^{-/-}$ cells failed to generate beating CMs and yielded close to 0% cTnT^{+} CMs when examined by flow cytometry (Figure 1B, C). In contrast, *GATA6*$^{+/-}$ hESCs did generate beating CMs (~25% cTnT^{+}) but at a significantly reduced efficiency compared to WT cells (~55% cTnT^{+}, Figure 1B, C). *GATA6*$^{+/-}$ CMs obtained were comparable morphologically to WT CMs with no obvious sarcomere defects (Supplemental Figure 1D). No significant differences in %cTnT^{+} were observed between clones of the same genotype (Figure 1C), therefore data from lines with the same genotypes were combined in all subsequent comparisons.

We also generated an iPSC line derived from a CHD patient presenting with an atrial septal defect and congenital diaphragmatic hernia; this patient was found to have a heterozygous frameshift mutation in *GATA6* (c.1071delG)[15]. The mutant allele was corrected to WT sequence (*GATA6*$^{corr/+}$) using CRISPR-Cas9 gene editing (Supplemental Figure 1E, F). The iPSC colonies expressed normal levels of the pluripotency markers NANOG and SOX2 demonstrating efficient reprogramming (Supplemental Figure 1G). *GATA6*$^{1071delG/+}$ cells generated cTnT^{+} CMs less efficiently than *GATA6*$^{corr/+}$ cells, on average about 50% (Supplemental Figure 1H), indicating that the *GATA6* c.1071delG mutation similarly disrupts cardiac differentiation as observed in the hESC heterozygous mutant lines. Likewise, the CMs obtained by differentiation of either *GATA6*$^{1071delG/+}$ or *GATA6*$^{corr/+}$ iPSCs appeared morphologically normal (Supplemental Figure 1I). The corrected iPSC line was shown to have

a grossly normal karyotype and to restore higher levels of GATA6 protein as expected (Supplemental Figure 1J, K).

GATA6 is required for CPC specification

The impaired CM generation from *GATA6* mutant hESCs may be due to deficient CPC specification. Therefore, RT-qPCR assays were performed on *GATA6*$^{+/-}$, *GATA6*$^{-/-}$ and WT cells harvested at day 6 of cardiac differentiation to examine the expression levels of the CPC markers *NKX2.5*, *TBX5*, *TBX20*, and *GATA4*. CPC marker expression levels were significantly reduced in *GATA6*$^{+/-}$ and *GATA6*$^{-/-}$ cells relative to WT controls, indicating a defect in CPC specification (Figure 1D). At this time point here was a clear trend but not a statistically significant difference in the expression levels of CPC markers comparing the *GATA6*$^{+/-}$ and *GATA6*$^{-/-}$ genotypes. However, an RT-qPCR time course showed that CPC marker expression level was increased (although not to WT levels) in *GATA6*$^{+/-}$ cells at later stages (days 8 to 11) while *GATA6*$^{-/-}$ CPC gene expression levels remained "flat" in comparison with no increase over time (Supplemental Figure 2A).

GATA6$^{+/+}$, *GATA6*$^{+/-}$, and *GATA6*$^{-/-}$ hESCs were differentiated toward the CM lineage using an alternative protocol based on chemical manipulation of the WNT pathway[29] (CHIR protocol, Supplemental Figure 2B). We observed the same phenotype in *GATA6*$^{-/-}$ cells and *GATA6*$^{+/-}$ cells using the CHIR protocol as with the cytokine-based protocol (data not shown), consistent with a previous report[19]. Bulk RNA-seq was performed at day 5 using the CHIR protocol (Supplemental Figure 2C-E). Principal component analysis (PCA) showed that the cells derived from each genotype were well separated from each other (Supplemental Figure 2C). Differential gene expression and gene ontology (GO) analyses revealed that *GATA6*$^{-/-}$ cells had strongly reduced expression levels of cardiac development related gene sets including "OFT septum morphogenesis" and "heart development" compared to WT controls (Supplemental Figure 2D). Furthermore, while *GATA6*$^{+/-}$ cells had relatively higher expression levels for many of these genes compared to *GATA6*$^{-/-}$ cells, numerous CPC regulatory genes showed decreased levels compared to WT controls (including *NKX2.5*, *TBX20*, *TBX5*, *MEF2C*, and *HAND2*; Supplemental Figure 2E) confirming an impairment of CPC development in differentiating *GATA6* mutant hESCs. GO analysis of genes with increased expression levels in *GATA6*$^{-/-}$ cells relative to WT included gene sets such as "nervous system development" (Supplemental Figure 2D) suggesting the adoption of a non-

cardiac genetic signature. Notably, gene sets related to retinoic acid (RA) signaling were significantly increased in GATA6$^{-/-}$ cells relative to WT (Supplemental Figure 2D), and *ALDH1A2* expression (the main enzyme that generates RA) was increased in *GATA6*$^{-/-}$ cells relative to WT from days 4 to 6 using the cytokine-based protocol (Supplemental Figure 2F), consistent with a previous study of cardiac differentiation using *GATA6* loss-of-function hiPSCs[19]. Proper RA signaling is crucial for cardiogenesis including OFT development and cardiac chamber morphogenesis[30], and inhibiting excessive RA signaling in *GATA6* mutant hiPSCs was shown to partially rescue CPC marker expression[19]. Thus, upregulated RA signaling in *GATA6*$^{-/-}$ hESCs during the CPC developmental stage may partially underly the CM differentiation defects.

GATA6 loss-of-function disrupts cardiac mesoderm patterning

Examining protein expression at multiple stages during cardiac differentiation revealed the earliest (and highest) expression level for GATA6 at day 2 of differentiation (Figure 2A). The impaired CPC development in *GATA6*$^{+/-}$ and *GATA6*$^{-/-}$ cells may therefore be due to defective cardiac mesoderm patterning during the early stages of cardiogenesis. We examined co-expression of the precardiac mesoderm markers KDR and PDGFRα (KP)[27] using flow cytometry from day 3 to 5 of cardiac differentiation (Figure 2B). At day 3, there was no significant difference in the %K^+P^+ cells between genotypes (~45% K^+P^+), but by day 5 the %K^+P^+ increased to ~72% in WT and *GATA6*$^{+/-}$ cells, while the %K^+P^+ was markedly reduced in *GATA6*$^{-/-}$ cells (~22%, Figure 2B, C). This is consistent with previous reports where sorting and reseeding K^+P^+ cells at day 3 of cardiac differentiation generated both mesenchymal cells and CMs but day 5 sorted K^+P^+ cells gave rise predominantly to CMs, indicating that day 5 KP expression is relatively enriched for precardiac mesoderm[27,31]. *GATA6*$^{+/-}$ cells had a small but significant decrease in the %K^+P^+ cells at day 4 relative to WT (Supplemental Figure 3A, B) suggesting that the developing K^+P^+ cardiac mesoderm in *GATA6*$^{+/-}$ cells is temporarily defective or delayed relative to WT controls. Notably, the decreased %K^+P^+ observed at day 4 (*GATA6*$^{+/-}$ and *GATA6*$^{-/-}$ cells) and day 5 (*GATA6*$^{-/-}$ cells) relative to WT cells was due to reduced KDR but not PDGFRα expression (Figure 2D, E, Supplemental Figure 3A, B), indicating that KDR is (directly or indirectly) regulated by GATA6 during cardiac mesoderm patterning.

We next sought to determine whether GATA6 loss-of-function impaired mesoderm induction by analyzing the expression of the pan-mesoderm marker BRACHYURY (*T*). Flow cytometry performed on WT, *GATA6*$^{+/-}$, or *GATA6*$^{-/-}$ cells at day 2 or 3 of cardiac differentiation revealed no significant difference in abundance of BRACHYURY^{+} cells between genotypes (Figure 2F, G). Likewise, there was no significant change in *T* or the mesendoderm marker *EOMES* transcript levels at day 2 when assessed by RT-qPCR (Figure 2H, I). These results indicate that *GATA6* mutant hESCs have the capacity to differentiate into a nascent mesendoderm/early mesoderm population that is deficient in patterning cardiac mesoderm.

Transcriptome analysis of *GATA6* mutant hESCs during early mesoderm patterning

During gastrulation, sequentially lineage-restrictive mesodermal cell populations emerge along a developmental trajectory involving primitive streak to lateral mesoderm formation, followed by cardiac mesoderm patterning[32]. As *GATA6* loss-of-function hESCs differentiated to an emergent mesendoderm/mesoderm stage but failed to properly generate cardiac mesdoderm, we hypothesized that GATA6 is required during the earliest stages of lateral and precardiac mesoderm patterning. GATA6-regulated genes important during these early mesoderm patterning stages were investigated by performing bulk RNA-seq at day 2 or day 3 of cardiac differentiation (Supplemental Figure 4A, B). Again, PCA showed the profiles representing each genotype were well separated. GO analysis and gene set enrichment analysis (GSEA) using the biological process (BP) subcollection for differentially expressed genes (DEGs; defined as p-adj<0.05 and $\log_2$(fold change)>0.5) comparing *GATA6*$^{-/-}$ to WT samples revealed decreased enrichment for GO terms including “heart development” (e.g., *HAND1*) and “OFT septum morphogenesis” (e.g., *NRP1*) at days 2 and 3 suggesting a disruption of early cardiac signature genes (Figure 3A, C, D). Conversely, GO analysis of increased DEGs in *GATA6*$^{-/-}$ samples relative to WT at days 2 and 3 included “extracellular matrix (ECM) organization”, “skeletal system development”, and “AP axis specification” (Figure 3B, D), suggesting that *GATA6*$^{-/-}$ cells are biased to other lineages such as paraxial mesoderm or retain an early mesodermal phenotype by day 3.

GATA6$^{+/-}$ samples also had reduced expression levels for genes associated with cardiac GO terms such as “cardiac muscle contraction” and “OFT septum morphogenesis” when comparing to WT controls at day 3 (Supplemental Figure 4C, D). Indeed, there was overlap for many of the decreased DEGs (dDEGs) observed in

GATA6$^{+/-}$ and *GATA6*$^{-/-}$ cells at day 2 or day 3 (relative to WT) including cardiac development genes such as *ERBB4* (important for endocardial cushion and ventricular trabeculae development[33]), the second heart field (SHF) related transcription factor *HAND2*, and the cardiac mesoderm marker *LRRC32*[34]; although the decrease in expression levels for these genes relative to WT was not as severe in the *GATA6*$^{+/-}$ genotype as for *GATA6*$^{-/-}$ (Supplemental Figure 4D, E, F).

We observed dysregulation of genes related to the WNT and BMP networks in *GATA6*$^{-/-}$ samples relative to WT at day 2 (Supplemental Figure 4G) and GO and GSEA analyses revealed decreased levels of "positive regulation of the BMP pathway" and increased levels of "negative regulation of canonical WNT pathway" at days 2 or 3 relative to WT (Figure 3A, B, D, E). Several dDEGs identified in *GATA6*$^{-/-}$ cells at day 2 or day 3 relative to WT samples included negative regulators of WNT signaling, including *SFRP1* and *TLE1* (Supplemental Figure 4E, G), and antagonists of the BMP pathway, such as *BMPER* and *SMAD6* (Figure 3A, E, Supplemental Figure 4E, G), indicating that the overall transcriptional response induced by the WNT and BMP pathways is dysregulated. *GATA6*$^{+/-}$ cells also exhibited perturbed gene expression for several WNT- and BMP-related genes (at an intermediate level to those observed in *GATA6*$^{-/-}$ cells) at days 2 or 3 relative to WT (Figure 3E, Supplemental Figure 4G). Mesoderm patterning is controlled by the input of WNT, BMP, and TGFβ signaling and dysfunction in these pathways cause severe developmental defects[35,36]. Therefore the cardiac defects caused by GATA6 loss-of-function may be caused by these alterations in WNT and BMP signaling.

We examined activity of the BMP, TGFβ and WNT pathways by analyzing the effector proteins SMAD1/5/9 (BMP activated), SMAD2/3 (TGFβ activated), and β-catenin (WNT activated) by western blotting at day 2. There was no change in the levels of active phospho-SMAD1/5/9, phospho-SMAD2/3, or non-phospho-β-catenin when comparing *GATA6*$^{+/-}$, *GATA6*$^{-/-}$ and WT cells (Figure 3F). These results indicate that GATA6 regulates the transcriptional response of genes activated by the BMP and WNT pathways downstream of canonical effector protein activation.

To further examine the impact of *GATA6* loss-of-function on early mesoderm patterning, we correlated RNA-seq data from a study examining hESC differentiation toward cardiac mesoderm[37] to our day 2 or day 3 RNA-seq data. GSEA analysis using increased DEGs at day 2 (lateral mesoderm) or day 3 (precardiac mesoderm) from Koh et al.[37] revealed significantly reduced enrichment in our *GATA6*$^{-/-}$ samples (relative to WT)

on days 2 or 3, respectively (Figure 3G, H). Furthermore, *GATA6*$^{+/-}$ cells had partially reduced expression for these lateral and precardiac mesoderm genes relative to WT cells (Figure 3H), suggesting that the impaired CPC and CM differentiation observed for *GATA6*$^{+/-}$ hESCs originates as disrupted lateral and cardiac mesoderm patterning.

A previous study of GATA6 function during DE differentiation from hESCs reported an interaction between GATA6, EOMES, and SMAD2/3 to co-regulate genes important during mesendoderm and transition to DE development[22]. DE and cardiac mesoderm originate from a bipotent germlayer mesendoderm population[38] and likely share a gene expression signature at this early stage. We therefore performed GSEA analysis using the CHIP-seq dataset for triple-overlap of GATA6, EOMES, and SMAD2/3 during early DE differentiation from Chia et al.[22] and found a significantly decreased enrichment in *GATA6*$^{-/-}$ cells relative to WT at day 2 (Supplemental Figure 4H). EOMES is an important transcriptional regulator of anterior mesoderm development[39], and as GATA6 was shown to interact with EOMES during early DE differentiation[22,40] we hypothesized that an interaction is similarly necessary during early lateral mesoderm patterning. We therefore performed GSEA using another published dataset of EOMES targets identified during mesoderm and DE (ME) differentiation in mouse ESCs (mESCs)[41]. GSEA analysis of our day 2 RNA-seq data with the "EOMES ME direct activation dataset" human gene equivalents revealed a significant decrease in enrichment in *GATA6*$^{-/-}$ cells relative to WT (Supplemental Figure 4H), supporting the notion that GATA6 cooperates with EOMES to co-regulate genes required for lateral mesoderm patterning.

GATA6 binds to putative regulatory regions associated with BMP, WNT, and EOMES related dDEGs

To determine the genomic localization of GATA6 occupancy during mesoderm patterning, we performed cleavage under targets and release using nuclease (CUT&RUN) sequencing for GATA6 at day 2 of differentiation using GATA6$^{+/+}$ hESCs. 1,273 significant differentially bound sites were identified for GATA6 relative to IgG control samples, associated with 953 transcriptional start sites (TSS) for unique genes (Figure 4A). Significant GATA6 binding sites predominately localized to intronic (46.03%) and distal intergenic (32.21%, >5kb from TSS) regions (Figure 4A), consistent with previous reports of GATA6 binding distribution[42,43]. Transcription factor binding motif enrichment analysis revealed the strongest enrichment at GATA6 bound loci for "GATA" motifs, as

well as “LHX-like” (LIM homeobox transcription factor; expressed in cardiac and other mesodermal derivatives[44]) and “EOMES” motifs (Figure 4B). GO analysis of the gene list nearby significant GATA6 binding peaks showed striking similarity to GO analysis from RNA-seq dDEGs in *GATA6*$^{-/-}$ cells (relative to WT), including “OFT septum morphogenesis”, “BMP signaling pathway” and “WNT signaling pathway” (Figure 4C). Additionally, we observed an overlap of CUT&RUN identified genes with day 2 (17.9%) and day 3 (16.8%) RNA-seq dDEGs in *GATA6*$^{-/-}$ cells (relative to WT) representing high likelihood direct targets of GATA6 including the cardiac development related genes *HAND1* and *MYOCD* (Figure 4D). Visualizing the localization of these GATA6 peaks that mapped to day 2 and day 3 dDEGs confirmed binding in intronic regions or at distal intergenic regions that overlapped with known enhancer-like signatures identified by the ENCODE Project[45] (Figure 4E). These included several WNT-related genes such as *MCC* and *LGR5*, as well as BMP-related genes including *SMAD6* (Figure 4E).

Day 2 GATA6 CUT&RUN data revealed an enrichment for binding to sequences containing EOMES motifs (Figure 4B). We compared our day 2 GATA6 CUT&RUN and RNA-seq data to previously published EOMES CHIP-seq data performed on hESCs at day 2 of DE differentiation[46]. Comparing these datasets revealed 32 genes that had triple-overlap of day 2 GATA6 CUT&RUN identified genes (953 genes nearby significantly bound sites), day 2 RNA-seq dDEGs, and EOMES CHIP-seq targets[46] (Figure 4F). Among this list of triple-overlap genes are known cardiac development factors including *LGR5*, which was reported to be required for hESC-CM differentiation[47], and *PRDM1*, which is expressed in the SHF and involved in OFT morphogenesis[48]. Visualizing the location of these triple-overlap genes confirmed that the GATA6 peaks directly overlapped with many EOMES CHIP-seq peaks (Supplemental Figure 5), suggesting that GATA6 and EOMES interact to co-regulate genes required for precardiac mesoderm patterning.

GATA6 interactome analysis during precardiac to cardiac mesoderm patterning stages

We next analyzed the GATA6 interactome using rapid immunoprecipitation of endogenous proteins (RIME) on WT cells at day 2 or day 4 of cardiac differentiation to define the chromatin associated protein interactions. 99 significant interacting proteins at day 2 and 52 unique proteins at day 4 of cardiac differentiation were identified bound to GATA6 compared to IgG control samples (Figure 5A). EOMES was one of the most enriched proteins bound to GATA6 at day 2 but was not identified in the day 4 GATA6-RIME analysis (Figure 5B). 81.8% of proteins

identified by GATA6-RIME at day 2 were not encoded by significantly differentially expressed genes identified by day 2 RNA-seq (*GATA6*$^{-/-}$ vs. WT) while 18.2% were, including TLE1, VRTN, and ZIC2 (Supplemental Figure 6A), indicating that GATA6 functions in parallel with most interacting proteins identified. Many of the significantly bound proteins were components of chromatin remodeling complexes such as members of the SWI/SNF complex (e.g., SMARCC1, SMARCA4, and ARID1A), which functions to mobilize nucleosomes and promote DNA accessibility[49], and the Nucleosome Remodeling and Deacetylase (NuRD) complex (e.g., KDM1A, MTA1/2/3, and GATAD2A), a chromatin remodeling complex associated with transcriptional repression[50] (Figure 5B). GATA6 protein interactions were also observed for other epigenetic and transcriptional regulators including those related to histone deacetylation (i.e., HDAC2) and mRNA splicing (i.e., SF1, Figure 5B, D). Interestingly, WNT/β-catenin transcriptional regulators were identified bound to GATA6, particularly at day 2 of cardiac differentiation, including the β-catenin transcriptional co-activator EP300[51], and the TCF/LEF transcriptional co-repressors CTBP1/2[52,53] and TLE1[54] (Figure 5B), suggesting that GATA6 may directly modulate the transcriptional response induced by WNT signaling by binding to these proteins.

Proteins identified by GATA6-RIME only at day 2 included the transcription factors EOMES and MIXL1 (both transcription factors involved in primitive streak formation and mesoderm patterning[34,55]) as well at TLE1, EP300 and SMARCA5, while the unique day 4 proteins were all RNA binding proteins such as TAF15 (Figure 5C). The overlapping day 2 and day 4 GATA6-RIME results included many chromatin remodelers such as SMARCC1, SMARCA4 and KDM1A (Figure 5C), although the enrichment for these proteins was greater at day 2 compared to day 4 (Figure 5B, Supplemental Table 1). As day 2 of differentiation had the highest level of GATA6 expression and enrichment for RIME identified proteins, we performed GATA6 immunoprecipitation (IP) on *GATA6*$^{+/+}$ and *GATA6*$^{-/-}$ samples at day 2 and confirmed a weak interaction with EOMES and SMARCC1 in the WT samples, with no observable bands in *GATA6*$^{-/-}$ samples (Figure 5E). The EOMES and SMARCC1 protein bands identified in GATA6-IP samples were notably less than observed for the input controls, therefore it's possible that the interaction between GATA6 and these proteins is indirect (i.e., GATA6 may be co-bound in a complex with EOMES and/or SMARCC1 among other proteins).

Previous studies performed GATA6-RIME at day 4 and EOMES-RIME at day 2 of DE differentiation[21,40], so we compared our day 2 and day 4 GATA6-RIME data to these previously published RIME datasets

(Supplemental Figure 6B). 26 proteins were present in all 4 datasets (Supplemental Figure 6B, C), implying there is a common interaction between GATA6 and various remodeler proteins, the transcription factor SALL4, and the TCF/LEF co-repressors CTBP1/2 during mesendoderm patterning toward both cardiac mesoderm and DE lineages. Protein interactions unique to day 2 GATA6- and EOMES-RIME included MIXL1, SMARCC2, and ARID1B and may represent protein interactions specific to mesendoderm development (Supplemental Figure 6C). Notably, EOMES and the WNT-related proteins TLE1 and EP300 were not identified in our day 4 dataset but were present in our day 2 GATA6-RIME data and the published EOMES and GATA6-RIME datasets during early DE development[21,40]. Therefore, an interaction between GATA6 and these proteins appears to be relinquished by the cardiac mesoderm stage (day 4) but persists during DE patterning. Cardiac differentiation requires a transient inhibition of the canonical WNT signaling pathway[56], and as day 4 of our cardiac differentiation protocol occurs after WNT inhibition these varying protein interactions may reflect the differing contributions of the WNT pathway during cardiac and DE differentiation.

Early manipulation of the WNT and BMP pathways partially rescues the CM defects in GATA6 mutant hESCs

LGR5, a component of the WNT pathway[57], was among the most significant dDEGs identified from day 2 or day 3 RNA-seq in GATA6$^{-/-}$ cells (relative to WT) and was also found significantly bound by GATA6 (and in a previous study, EOMES[46]) in WT cells (Supplemental Figure 5). As LGR5 is required for efficient CM differentiation in hPSCs[47,58], we hypothesized that infection with a doxycycline (DOX) inducible *LGR5*-expressing lentivirus might rescue the cardiac defects in *GATA6*$^{-/-}$ hESCs. In *GATA6*$^{-/-}$ hESCs that had been transduced with the inducible-*LGR5* lentivirus (i*LGR5*), DOX was added from days 1 to 4 of cardiac differentiation (Figure 6A) to mimic the *LGR5* expression pattern (Supplemental Figure 7A); we validated that this increased *LGR5* expression in a DOX-dose-dependent manner (Supplemental Figure 7B). In all differentiation experiments using i*LGR5* treated with DOX (250ng/mL), we did not observe generation of beating CMs. However, DOX treatment of i*LGR5*-transduced *GATA6*$^{-/-}$ hESCs did yield a small but significant increase in the %K^{+}P^{+} population at day 5 of differentiation relative to empty vector (EV) transduced controls, associated with increased KDR expression (Figure 6B). Thus,

LGR5 expression can partially rescue a proportion of day 5 cardiac mesoderm in *GATA6*$^{-/-}$ hESCs but cannot sufficiently improve subsequent CM differentiation.

As LGR5 is a single component of the complex WNT pathway, we tested a broader pharmacological approach by using the WNT agonist CHIR to determine if early WNT activation could more efficiently rescue the cardiac defects in *GATA6*$^{-/-}$ hESCs. We found that inclusion of CHIR (3μM) from days 0 to 2 in differentiating *GATA6*$^{-/-}$ hESCs yielded by day 13 small clusters of beating CMs (Supplemental Video 1). When assessing quantitatively by flow cytometry the %cTnT^{+} CMs in CHIR-treated *GATA6*$^{-/-}$ cells relative to vehicle treated controls, there was a variable trend for CM induction that was however not statistically significant (Supplemental Figure 7C). Similarly, while the %K^{+}P^{+} cardiac mesoderm cells at day 5 was slightly increased upon CHIR treatment in *GATA6*$^{-/-}$ cells, this was not a statistically significant improvement (Supplemental Figure 7D).

BMP-related gene expression was also dysregulated at day 2 in *GATA6*$^{-/-}$ cells and thus manipulation of the BMP4 concentration in combination with CHIR treatment from days 0 to 2 was tested to further promote CM rescue. Interestingly, we found that decreasing the BMP4 concentration (5ng/mL) combined with CHIR treatment yielded small clusters of beating CMs (Supplemental Video 2) more consistently than increasing the BMP4 concentration (data not shown) or treatment with CHIR on its own. Quantification by flow cytometery for %cTnT^{+} CMs in *GATA6*$^{-/-}$ cells treated with CHIR and the lower BMP4 concentration (CHIR LB) showed a small but significant increase (~4% cTnT^{+}) relative to *GATA6*$^{-/-}$ controls indicating that CM differentiation is partially rescued upon CHIR LB treatment (Figure 6C). The %K^{+}P^{+} and %K^{+} day 5 cardiac mesoderm population was also significantly increased with CHIR LB treatment in *GATA6*$^{-/-}$ cells relative to untreated controls and was not significantly different than WT controls indicating a rescue of day 5 K^{+}P^{+} cardiac mesoderm (Figure 6D). Taken together, these results indicate that modulating the early input of the WNT and BMP pathways in *GATA6*$^{-/-}$ cells can rescue the cardiac mesoderm patterning defects and partially rescue subsequent CM differentiation.

GATA6$^{+/-}$ cells also exhibited partial dysregulated gene expression related to WNT signaling via day 2 RNA-seq relative to WT controls (Supplemental Figure 4G). We therefore hypothesized that the addition of CHIR from days 0 to 2 in differentiating *GATA6*$^{+/-}$ hESCs could rescue CM differentiation more potently than observed in *GATA6*$^{-/-}$ hESCs. Indeed, we found that the %cTnT^{+} CMs was significantly increased in *GATA6*$^{+/-}$ cells supplemented with CHIR relative to vehicle treated controls and was not significantly different from WT untreated

controls, indicating an efficient rescue of CM differentiation (Figure 6E). CHIR addition to WT hESCs had a deleterious effect on CM differentiation efficiency, with the %cTnT^{+} CMs reduced from ~60% (DMSO treated) to ~25% (CHIR treated, Figure 6E), suggesting that there is a threshold "window" for the degree of WNT pathway activation required during early primitive streak to mesoderm patterning stages and that reducing or exceeding this threshold has an adverse effect on later CM differentiation capacity. Furthermore, this data indicates that the rescue in CM differentiation efficiency in *GATA6*$^{+/-}$ cells treated with CHIR was not due to an overall improvement in the general cardiac differentiation protocol, but rather related to correcting the consequence of loss of one *GATA6* allele.

Discussion

We found that *GATA6* loss-of-function mutations severely disrupt CPC gene expression and impair CM differentiation, consistent with the results described by Sharma et al.[19]. Here, we discovered that GATA6 is required very early in this process and that the later cardiac phenotypes observed in *GATA6*$^{+/-}$ and *GATA6*$^{-/-}$ hESCs originate from an early mesoderm patterning defect in which lateral and cardiac mesoderm genes fail to be expressed at normal levels. Gene networks induced by the WNT and BMP pathways that are normally required for primitive streak organization and subsequent anterior lateral mesoderm emergence are also mis-expressed when GATA6 is deficient. GATA6 CUT&RUN analysis revealed binding at distal enhancer-like signatures nearby dDEGs identified by RNA-seq, and GATA6 binding was found to have a considerable overlap with previously published EOMES CHIP-seq data during early DE differentiation[46] nearby many of these genes. Day 2 GATA6 RIME analysis confirmed binding with EOMES and various chromatin remodelers including components of the SWI/SNF and NuRD remodeling complexes that are known to regulate chromatin accessibility of cardiac lineage-specific gene networks[59-63]. Furthermore, we found that early manipulation of the WNT pathway through CHIR treatment from days 0 to 2 rescued CM defects observed in *GATA6*$^{+/-}$ hESCs while CHIR treatment and reduced BMP4 dosage rescued K^{+}P^{+} cardiac mesoderm and partially rescued CM differentiation in *GATA6*$^{-/-}$ hESCs. Together, these results present multiple novel functions for GATA6 in regulating early precardiac mesoderm patterning during human cardiac differentiation.

WNT and BMP related genes were dysregulated in *GATA6*$^{+/-}$ and *GATA6*$^{-/-}$ cells at day 2 and day 3 of cardiac differentiation but β-catenin and SMAD protein activation was intact indicating that the transcriptional response of these pathways is defective rather than the upstream activation induced by morphogens. GATA6 RIME analysis revealed an interaction with several WNT transcriptional regulators including the β-catenin co-activator EP300 and the TCF/LEF transcriptional co-repressors TLE1 and CTBP1/2, and binding to these proteins could have positive or negative effects on their function. One potential mechanism is that GATA6 binds to these WNT regulators and prevents their repressive (or in the case for EP300, potentiating) function on TCF-mediated transcription, causing a net increase in the β-catenin transcriptional response. Indeed, there was an enrichment for negative regulation of the WNT signaling pathway at day 2 in *GATA6*$^{-/-}$ cells according to RNA-seq data, suggesting that GATA6 loss-of-function increases feedback inhibition of TCF/LEF-mediated transcription. GATA6 CUT&RUN analysis also revealed binding near many genes related to WNT and BMP signaling implying direct participation in modulating appropriate β-catenin/SMAD transcriptional responses. However, many WNT/BMP response genes dysregulated in *GATA6*$^{+/-}$ and *GATA6*$^{-/-}$ cells were not identified as targets by GATA6 CUT&RUN, suggesting that another method for regulation is indirect, perhaps related to the interaction with chromatin remodelers affecting DNA accessibility.

RIME analysis revealed GATA6 bound to many chromatin remodelers including components of the SWI/SNF (e.g., SMARCA4) and NuRD (e.g., KDM1A) complexes at days 2 and 4 of cardiac differentiation. GATA6 is a pioneer transcription factor with specialized function to bind and promote accessibility of chromatin during CPC development[19], and GATA6, GATA4, and GATA3 have previously been shown to interact with various members of SWI/SNF complexes such as SMARCA4[19,21,64,65]. However, the molecular mechanism for how GATA6 modifies the accessibility of chromatin and mobilizes nucleosomes is unclear. The AP-1 pioneer factor interacts with SWI/SNF complexes to promote their localization to non-permissive regions of chromatin[66]. GATA6 may function similarly, for example, by binding to SWI/SNF complex proteins and recruiting them to regions of closed chromatin containing lineage-specific enhancers where they then function to promote genomic accessibility.

The function of GATA6 during early mesoderm patterning presented in this study has unique implications toward understanding the pathogenesis of CHD and extra-cardiac phenotypes associated with human *GATA6*

mutations. *GATA6* homozygous loss-of-function mutations have not been described in humans, most likely due to early embryonic lethality causing non-viable embryogenesis. This is consistent with the early mesoderm patterning defects of *GATA6*$^{-/-}$ hESCs described in this study, previous reports of DE defects in *GATA6*-null hPSC lines[20-23], as well as the early lethality reported in *GATA6* KO mice[7]. In the case of haploinsufficiency, CHD presenting as OFT or septal defects associated with heterozygous *GATA6* mutations may be due to defects that occur during early mesoderm patterning that diminish the later developmental pool of CPCs and CMs. Quite remarkably, profiles of cells at day 2 of differentiation already identify OFT morphogenesis as gene sets disturbed by loss of GATA6. Relatively minor changes in early mesoderm cell population numbers have recently been reported to associate with later heart defects in a mouse model of Cornelia de Lange syndrome using *NPBL1*$^{+/-}$ mice[67], and thus *GATA6* heterozygous mutations may similarly have a subtle negative effect on developing mesodermal cell populations to cause CHD. Human mutations in *GATA6* commonly associate with OFT defects, a primarily second heart field (SHF) derived structure, and recent work has established that SHF lineage progenitors are derived from early defined mesodermal subpopulations[68]. Therefore, *GATA6* mutations might impair specific heart field progenitor populations based on the timing and positioning of these developing mesodermal populations in the primitive streak, long before the progenitors are associated with SHF. *GATA6* haploinsufficiency in humans also associates with endoderm defects such as pancreatic agenesis, and DE and early mesoderm co-develop from a common mesendoderm population adjacent to one another in the anterior primitive streak during gastrulation[69]. Defects in the regulatory functions of GATA6 during mesendoderm patterning, such as interactions with EOMES and specific chromatin remodelers, may cause downstream organ defects in both mesoderm and endoderm derived organ systems in some patients with *GATA6* mutations.

Materials and Methods

hPSC Culture. hPSC lines were cultured on Matrigel (Corning BD354277) coated tissue culture plates using StemFlex (Thermo Fisher Scientific A3349401) or mTESR Plus (Stem Cell Technologies 1000276) medium at 37°C and 5% CO_2. Cells were passaged using Accutase Cell Detachment Solution (VWR 10761-312) and supplemented with 10 μM ROCK inhibitor (RI) Y-27632 (Selleckchem S1049) for one day. hPSCs were routinely

tested for mycoplasma contamination using the LookOut Mycoplasma PCR Detection Kit (Sigma-Aldrich MP0035).

iPSC generation. A skin biopsy was obtained from a patient with an atrial septal defect and congenital diaphragmatic hernia associated with a heterozygous frameshift mutation in *GATA6* (c.1071delG)[15]. Human dermal fibroblasts (HDF) derived from this biopsy were transduced with 4 Sendai viruses expressing OCT3/4, SOX2, KLF4, and c-MYC using the CytoTune-iPS 2.0 Sendai Reprogramming Kit (Invitrogen A16517). Transduced HDFs were reprogrammed on CF1 Mouse Embryonic Fibroblasts (MEFs) (Thermo Fisher Scientific A34180) with iPSC medium consisting of DMEM/F12 (VWR 16777-255) supplemented with 20% KnockOut serum replacement (KOSR, Thermo Fisher Scientific 10828010), 1% non-essential amino acids (Thermo Fisher Scientific), 1% L-glutamine (Corning 25-005-CI), 1% Penicillin:Streptomycin Solution (Corning 30-002-CI), 0.0007% 2-mercaptoethanol (Thermo Fisher Scientific 21985023), 10 ng/mL bFGF (R&D Systems 233-FB-025). Once iPSC colonies emerged, colonies were manually isolated and expanded into feeder-free conditions by culturing with mTESR1 (Stem Cell Technologies 85850) on Matrigel coated plates.

CRISPR Gene Editing. The GATA6 mutant H1 (WA01, NIH #0043) hESC cell lines were established in a previous study[20] using the H1-iCas9 cell line and CRISPR gene editing[28] targeting the C-terminal ZnF domain (Supplemental Figure 1A, B). The *GATA6* c.1071delG iPSC mutant allele was corrected to WT sequence to create the isogenic *GATA6*$^{corr/+}$ line (as well as unmodified *GATA6*$^{1071delG+}$ CRISPR-control clones) using CRISPR technology with Nickase-Cas9 according to previously established methods[70]. A pair of gRNA sequences were designed targeting opposing DNA strands surrounding the G deletion site. The gRNA 1 sequence was specifically designed to overlap the G deletion site to prevent Nickase-Cas9 activity on the WT *GATA6* allele. A 91 nucleotide (nt) length single-stranded DNA (ssDNA) repair template (Integrated DNA Technologies) was designed with 45 nt homology arms flanking the G mutation site, including a G to A silent mutation in the right homology arm and gRNA 2 recognition sequence to prevent Nickase-Cas9 activity after homology directed repair (HDR). gRNAs 1 and 2 (Supplemental Table 2) were cloned into the pSpCas9n(BB)-2A-Puro (PX462) V2.0 plasmid (Addgene 62987) as described previously[70]. 2 million dissociated *GATA6* c.1071delG/+ iPSCs were electroporated with 4 μg each gRNA-PX462 vector with 3 μL of 100 μmol/L ssDNA donor oligonucleotide using the Neon Transfection System (2 pulses at 1450V for 20 milliseconds, Invitrogen NEON1S) and plated on

Matrigel coated dishes with mTESR Plus supplemented with 10 μM RI. A T7 endonuclease I assay (New England Biolabs M0302S) was performed to quantify indel frequency of gRNA pairs following PCR amplification (Phusion Hot Start Flex DNA Polymerase, New England Biolabs M0535L) and agarose gel electrophoresis from genomic DNA isolated 2-3 days after electroporation using the DNeasy Blood & Tissue Kit (Qiagen 69506). 24 hr after electroporation, the culture medium was replaced with mTESR Plus supplemented with 0.5 μg/mL Puromycin (Sigma-Aldrich P8833) for antibiotic resistance selection for 48 hr. iPSCs were then dissociated with Accutase and plated at a low density (~3000 iPSCs per 10cm plate) on Matrigel coated dishes with mTESR Plus medium (with 10μM RI for the first 24 hr) and allowed to grow for about 2 weeks before iPSC colonies were manually isolated and plated into Matrigel coated 96 well plates and cultured with mTESR Plus. DNA was isolated from iPSC clones using QuickExtract DNA Extraction Solution (Biosearch Technologies QE09050), PCR amplification was performed using primers surrounding the mutation site (Supplemental Table 2) and Sanger sequencing was performed to verify gene editing (GENEWIZ). Karyotyping was performed by WiCell Research Institute (Madison, WI).

hPSC Cardiomyocyte Differentiation. A monolayer cytokine-based cardiac differentiation protocol was adapted from previously established methods (Figure 1A)[26,27]. Briefly, a "base medium" for cardiac differentiation was prepared using RPMI 1640 (Thermo Fisher Scientific 22400089) supplemented with 0.5x B27 (Thermo Fisher Scientific 17504044), 0.5 mM 1-Thioglycerol (Sigma-Aldrich M6145), 50 μg/mL L-Ascorbic acid (Sigma-Aldrich A4544), and 1x GlutaMAX (Thermo Fisher Scientific 35050061). The hPSCs were plated at ~$4x10^4$ cells/cm^2 and allowed to grow for 2 days before changing with "Day 0 medium" consisting of the "base medium" plus 20 ng/mL BMP4 (R&D Systems 314-BP-050), 30 ng/mL Activin A (R&D Systems 338-AC-050), 5 ng/mL bFGF (R&D Systems 233-FB-025), and 5 μL/mL Transferrin (Roche 10652202001). BMP4 was used at 10 ng/ml for iPSC differentiation. Approximately 55 hr later, the medium was changed with "Day 2 medium" consisting of "base medium" supplemented with 5 μM XAV-939 (Sigma-Aldrich X3004), 5 ng/mL VEGF (R&D Systems 293-VE-050), and 5 μL/mL Transferrin. The culture medium was changed on days 4 and 6 of cardiac differentiation with "base medium" supplemented with 5 ng/mL VEGF. From day 9 and later the culture medium was changed with "base medium" every 2-3 days. For a subset of experiments, 3 μM CHIR99021 (Stem Cell Technologies 72054) was included in the "Day 0 medium" and/or the concentration of BMP4 was reduced to 5 ng/mL (Figure

6C-E, Supplemental Figure 7C, D). An alternative CM differentiation protocol based on chemical manipulation of the WNT pathway[29] was used for a subset of experiments (CHIR protocol, Supplemental Figure B-E). For the CHIR protocol, hESCs were plated at ~$4x10^4$ cells/cm^2 and allowed to grow for 2 days in mTESR Plus before changing medium to RPMI 1640 with 1x B27 minus insulin (Thermo Fisher Scientific A1895601) and 6 μM CHIR99021 (Stem Cell Technologies 72054) for 24 hr. Medium was then changed to RPMI 1640 with 1x B27 minus insulin for another 24 hr, before changing medium on day 3 to RPMI 1640 with 1x B27 minus insulin and 5 mM IWP2 (Tocris 3533). On day 5, culture medium was changed to RPMI 1640 with 1x B27 minus insulin once more and starting on day 7 medium was changed to RPMI with 1x B27 every other day. CMs were purified using a lactate-selection protocol to prepare for immunocytochemistry by changing the differentiation medium on day 15 of the cytokine-based protocol to a lactate-selection medium consisting of RPMI 1640 lacking glucose (Thermo Fisher Scientific 11879020) supplemented with 5 mM Sodium L-lactate (Sigma-Aldrich L7022), 213 μg/mL L-ascorbic acid, and 500 μg/mL Human Albumin (Sigma-Aldrich A9731). Lactate-selection medium was refreshed on day 17 of differentiation, after which the medium was restored to “base medium” on day 19 and changed every 2 to 3 days prior to fixation.

Flow Cytometry. Cells were detached from culture plates using 0.5% Trypsin / 0.5mM EDTA (VWR 45000-664) or TrypLE Express Enzyme (Thermo Fisher Scientific 12605010) and resuspended in a FACS buffer consisting of PBS with 10% FBS (for cTnT staining) or 0.5% BSA (for live cell staining). Cells were fixed by pelleting at 300g and resuspended in 0.2% paraformaldehyde (PFA) for 25 min at RT before staining with primary antibody for cTNT (Thermo Fisher Scientific MA5-12960) in FACS buffer with 0.5% Saponin (Sigma-Aldrich S7900-25G) for 1 hr at RT, washed 3x in FACS buffer, and then stained for 1 hr at RT with FACS buffer plus Saponin containing secondary antibody (Invitrogen A21236). Live cells were used for staining the cell surface proteins KP by incubating with FACS buffer containing PE-conjugated KDR antibody (R&D Systems FAB357P-100) and APC-conjugated PDGFRa antibody (R&D Systems FAB1264A) or IgG control antibodies (R&D Systems IC002P, IC002A) for 30 min at RT, and then stained with SYTOX Green Dead Cell Stain (Thermo Fisher Scientific S34860) in FACS buffer for 5 min at RT. BRACHYURY flow cytometry was performed using the Foxp3 Transcription Factor Staining Buffer Set (eBioscience 00-5523-00) according to the manufacturer’s protocol using a PE-conjugated BRACHYURY antibody (R&D Systems IC2085P) or IgG control antibody (R&D Systems

IC108P). Flow cytometry was performed and analyzed using an Attune NxT Flow Cytometer (ThermoFisher Scientific) for fixed cells and a BD-Accuri C6 Flow Cytometer (BD Biosciences) for live cells.

RT-qPCR. RNA was isolated using the RNeasy Mini Kit (QIAGEN 74106) and reverse-transcribed using the SuperScript VILO cDNA Synthesis Kit (Invitrogen 11754250) according to the manufacturer's protocols. The qPCR reaction was prepared by mixing cDNA with LightCycler 480 SYBR Green Master mix (Roche 04887-352-001) and primers listed in Supplemental Table 2. RT-qPCR was performed using a LightCycler 480 Instrument II (Roche). Gene expression data was normalized to endogenous *HPRT* expression levels as a control for each sample.

Western Blotting. Whole cell lysates were prepared using RIPA Lysis Buffer (Thermo Fisher Scientific 89900) supplemented with 1x Protease/Phosphatase Inhibitor Cocktail (Cell Signaling Technology 5872S) and 1x Benzonase (Millipore 70664-3). Protein was quantified using the Pierce BCA Protein Assay Kit (Thermo Fisher Scientific 23225) and electrophoresed on NuPAGE 4 to 12% Bis-Tris Gels (Invitrogen NP0335BOX) before transferring to PVDF membranes (Bio-Rad 162-0177). Blots were washed with 1x TBS with 0.1% Tween-20 (TBST) and blocked using 5% IgG-free BSA (VWR RLBSA50). Primary antibodies (Supplemental Table 2) were added to blocking buffer and stained overnight at 4°C. Secondary antibody staining was performed for 1 hr at RT using HRP-conjugated antibodies (Supplemental Table 2) in blocking buffer. Pierce™ ECL Western Blotting Substrate (Thermo Fisher Scientific 32106) used used to visualize proteins, and imaging was performed using a C-DiGit Blot Scanner (LICOR) with ImageStudio (v5.2) and Adobe Photoshop (v25.9.1) software.

Co-Immunoprecipitation. Co-immunoprecipitation (Co-IP) was performed using the Pierce™ Crosslink Magnetic IP/Co-IP Kit (Thermo Fisher Scientific 88805) according to the manufacturer's protocol using cells at day 2 of cardiac differentiation. 7μg of the GATA6 antibody (Cell Signaling Technology 5851) was used to cross-link to the Protein A/G Magnetic beads and 1 mg of protein was used for the IP reaction performed overnight at 4°C on a rotating platform. GATA6 Co-IP samples were electrophoresed on a gel and imaged as described for Western Blotting using 30 μg of protein lysate from the Co-IP used as an input control. *GATA6*$^{-/-}$ cell samples served as a negative control.

Immunocytochemistry and microscopy. Cells were fixed in tissue culture dishes with 4% PFA for 20 min at RT. Cells were washed in PBS and then blocked for 1 hr at RT with blocking buffer consisting of PBS with 10%

FBS, 0.1% IgG-free BSA (Rockland Immunochemicals BSA-10), 0.1% Saponin, and 10% goat serum (Jackson ImmunoResearch Laboratories Inc. 005-000-121). Cells were then stained with primary antibodies (Supplemental Table 2) diluted in blocking buffer (without goat serum) overnight at 4°C. Secondary antibody staining was performed in blocking buffer (without goat serum) for 1 hr at RT. Cells were stained with DAPI to visualize nuclei and imaged using a Zeiss LSM800 laser scanning confocal microscope with ZEN imaging software or a Zeiss Epifluorescence microscope with AxioVision software, and edited using Adobe Photoshop software (v25.9.1). Videos were taken using an Infinity5 Microscope Camera (Teledyne Lumenera) with Infinity Analyze software.

Lentivirus production and infection. *LGR5* full length cDNA was first cloned into a DOX-inducible Lentiviral vector containing a GFP selection marker (CS-TRE-PRE-Ubc-tTA-I2G[71]) by performing PCR for LGR5 using WT cDNA samples from day 2 of cardiac differentiation and primers designed to incorporate the BsiWI and MfeI restriction enzyme recognition sites flanking LGR5 (Supplemental Table 2) to allow digestion and insertion into the CS-TRE-PRE-Ubc-tTA-I2G vector. *LGR5* sequence was validated by Sanger sequencing (GENEWIZ) using sequencing primers listed in Supplemental Table 2. Lentivirus production was performed by transfecting 293T cells with the lentiviral expression vectors (LGR5 or EV control) and packaging plasmids using PEI. Transfected 293T cells were then allowed to produce lentivirus for 48 hr before the medium was collected, and the virus was concentrated using Lenti-X Concentrator (Takara 631231) according to the manufacturer's protocol and resuspended in StemFlex medium. *GATA6*$^{-/-}$ hESCs were infected with lentivirus by replacing medium with i*LGR5* or EV control[72] lentivirus concentrate in StemFlex for 16 hr before changing to normal StemFlex and seeded for 2 to 3 days. Lentivirus infected hESCs were then sorted based on GFP expression using FACS through the Weill Cornell Medicine Flow Cytometry Core Facility. Doxycline (DOX, Sigma-Aldrich D9891) was added from days 1 to 4 to induce expression of i*LGR5* or EV infected *GATA6*$^{-/-}$ hESCs.

RNA-seq. Total RNA was extracted from hESCs approximately 52 hr (day 2) or 74 hr (day 3) after starting the cardiac differentiation protocol using the RNeasy Mini Kit (QIAGEN 74106) from at least two independent biological replicates per sample. Total RNA integrity was verified using a 2100 Bioanalyzer (Agilent Technologies), and RNA concentrations were measured using the NanoDrop system (Thermo Fisher Scientific). Libraries were generated from day 2 RNA using the TruSeq RNA Library Prep Kit v2 (Illumina RS-122-2001)

and day 3 RNA using the TruSeq Stranded mRNA Library Prep Kit (Illumina 20020594) according to the manufacturer's instructions. Normalized cDNA libraries were pooled and sequenced on Illumina HiSeq4000 (Day 2, single read) or Illumina NovaSeq 6000 (Day 3, paired-end read) sequencing systems for 50 cycles through the Weill Cornell Medicine Genomics Resources Core Facility. The raw sequencing reads in BCL format were processed through bcl2fastq 2.19 (Illumina) for FASTQ conversion and demultiplexing. Day 2 RNA-seq alignment (GRChg19) and differential gene expression analysis was performed as described[73]. Day 3 RNA-seq reads were aligned and mapped to the GRCh38 human reference genome by STAR (Version 2.5.2[74]) and transcriptome resconstruction was performed by Cufflinks (Version 2.1.1, http://cole-trapnell-lab.github.io/cufflinks/) after trimming adaptors with cutadapt (Version 1.18, https://cutadapt.readthedocs.io/en/v1.18/). The abundance of transcripts was measured with Cufflinks in Fragments Per Kilobase of exon model per Million mapped reads (FPKM)[75,76]. Raw read counts per gene were extracted using HTSeq-count v0.11.2[77]. Gene expression profiles were constructed for differential expression, cluster, and principle component analyses with the DESeq2 package[78]. For differential expression analysis, pairwise comparisons between two or more groups using parametric tests where read-counts follow a negative binomial distribution with a gene-specific dispersion parameter were performed. Corrected p-values were calculated based on the Benjamini-Hochberg method to adjust for multiple testing. GSEA was performed using GSEA 4.2.3 software (Broad Institute, Inc. and Regents of the University of California)[79] on RNA-seq gene lists ranked by $\log_2$(Fold Change) using the subcollection of biological process (BP) gene sets from the GO collection in the Human Molecular Signatures Database (MSigDB)[80], or using custom gene lists from published sequencing datasets as described in this manuscript[22,37,41], and gene sets with a FDR (False Discovery Rate) q-value < 0.25 and a nominal p-value < 0.05 were considered to be enriched significantly. GO analysis was performed using the Database for Annotation, Visualization, and Integrated Discovery (DAVID, david.ncifcrf.gov)[81,82] using the BP subcollection. Heatmaps were generated from normalized counts from selected gene lists using SRplot (bioinformatics.com.cn/srplot)[83]. Differentially expressed genes (DEGs) were defined as p-value adjusted (p-adj) <0.05 and $\log_2$(fold change)>0.5, genes with a count below 50 for all samples were excluded.

CUT&RUN. 500,000 H1-*GATA6*$^{+/+}$ cells were harvested approximately 52 hr after starting the cardiac differentiation protocol and CUT&RUN was performed using the CUTANA ChIC/CUT&RUN Kit (Epicypher 14-1048) according to the manufacturer's protocol. Anti-GATA6 (n=3 independent biological replicates) (Cell

Signaling Technology 5851) and Rabbit Anti-IgG (n=2 independent biological replicates) negative control (Epicypher 13-0042) antibodies were used at a 1:50 dilution (~0.5μg). DNA libraries were generated using the 2S Library Kit (Swift) and sequenced using a NextSeq500 Sequencing System (Illumina) through the Weill Cornell Medicine Epigenomics and Genomics Core Facilities. FASTQ files were aligned to the GENCODE GRChg38 build of the human genome using bowtie2 with the –dovetail parameter. The resulting BAM files were sorted and indexed using samtools. The sorted and filtered BAM files were then converted to bedgraph format using bedtools and peaks were called using SEACR calling enriched regions in target data by selecting the top 1% of regions by AUC (stringent threshold). Transcription factor motif enrichment analysis was performed using Basepair software with HOMER following MACS2 peak calling (basepairtech.com). EOMES CHIP-seq data from Teo et al.[46] was aligned to GRChg38 using bowtie2 with Partek software (partek.com). CUT&RUN and CHIP-seq data were visualized using Integrative Genomics Viewer (IGV) 2.16.2, distal enhancer-like signatures (dELS) defined by the ENCODE project[45] were identified using the UCSC Genome Browser for hg38 (genome.ucsc.edu).

RIME analysis. About ~50 million H1-*GATA6*$^{+/+}$ cells at day 2 or day 4 of cardiac differentiation were fixed with 1% formaldehyde (Electron Microscopy Sciences 15710) for 8 min at RT with gentle agitation. Fixation was quenched with 125 mM glycine (Bio-Rad 1610718) for 5 min at RT before cells were manually scraped, transferred to conical tubes, and pelleted at 800g at 4°C for 10 min. Pellets were resuspended in PBS with 0.5% IGEPAL CA-630 (Sigma-Aldrich I8896) and centrifuged again before resuspending in PBS-IGEPAL with 1 mM PMSF (Thermo Fisher Scientific 36978) and centrifuged one final time. Supernatant was then removed from pellets which were then snap frozen on dry ice and transferred to -80°C. RIME analysis was performed by Active Motif (Carlsbad, CA) according to published methods[84] using 150 μg of chromatin per sample immunoprecipitating with anti-GATA6 (Cell Signaling Technology 5851) or anti-IgG control (Cell Signaling Technology 2729) antibodies (15 μg antibody per IP) and performing mass spectrometry with enriched GATA6 bound proteins defined as not present in the IgG controls and having a spectral count (the total number of all peptides detected) of at least 5 and >1 unique peptides.

Statistical analysis. Data is represented as the mean ± SEM from independent biological replicates (as indicated in figure legends). Graphing and statistical analysis was performed using GraphPad Prism v.10.2.3

software with two-tailed Student's t test when comparing two groups. One-way or two-way ANOVA was performed when comparing three or more groups, unless otherwise indicated.

Acknowledgements

JAB, DH, and TE conceived and planned the study. JAB generated most of the data, generated figures, and wrote the first manuscript draft. MG and KMB provided significant assistance and consult on experimental strategies and bioinformatics. RK and ZS generated and validated the iPSC lines. NdS and EY carried out experiments. ZS, KL, and DY generated and provided the hESC mutant lines prior to publication, and provided significant consult. WKC provided patient-derived fibroblasts used for iPSC generation. All authors edited and agreed on the final manuscript version. This work was supported by grants from the National Institutes of Health to TE (R35HL135778), DH (R01DK096239), and WKC (P01HD068250), an NIH postdoctoral fellowship to JAB (F32HL152575), the MSK Cancer Center Support Grant/Core Grant (P30CA008748), the Tri-Insitutional Medical Scientist Training Program to KMB (T32GM007739) and additional grants (TE and DH) from the Starr Tri-I Stem Cell Initiative (2016-004) and the New York State Department of Health (NYSTEM, C029567).

Competing interests

T.E. is a co-founder of OncoBeat, LLC.

Data availability

All RNA-seq and CUT&RUN data is available at the GEO repository and are publicly available as of the date of publication. The series accession number is GSExxxxxx. Requests for primary data, resources and reagents should be directed to and will be fulfilled by the lead contact, Todd Evans (tre2003@med.cornell.edu).

References

1. Hoffman JI, Kaplan S. The incidence of congenital heart disease. *J Am Coll Cardiol*. 2002;39:1890-1900. doi: 10.1016/s0735-1097(02)01886-7
2. Woudstra OI, Ahuja S, Bokma JP, Bouma BJ, Mulder BJM, Christoffels VM. Origins and consequences of congenital heart defects affecting the right ventricle. *Cardiovasc Res*. 2017;113:1509-1520. doi: 10.1093/cvr/cvx155
3. Patient RK, McGhee JD. The GATA family (vertebrates and invertebrates). *Curr Opin Genet Dev*. 2002;12:416-422. doi: 10.1016/s0959-437x(02)00319-2
4. Peterkin T, Gibson A, Patient R. Redundancy and evolution of GATA factor requirements in development of the myocardium. *Dev Biol*. 2007;311:623-635. doi: 10.1016/j.ydbio.2007.08.018
5. Molkentin JD. The zinc finger-containing transcription factors GATA-4, -5, and -6. Ubiquitously expressed regulators of tissue-specific gene expression. *J Biol Chem*. 2000;275:38949-38952. doi: 10.1074/jbc.R000029200
6. Peterkin T, Gibson A, Loose M, Patient R. The roles of GATA-4, -5 and -6 in vertebrate heart development. *Semin Cell Dev Biol*. 2005;16:83-94. doi: 10.1016/j.semcdb.2004.10.003
7. Morrisey EE, Tang Z, Sigrist K, Lu MM, Jiang F, Ip HS, Parmacek MS. GATA6 regulates HNF4 and is required for differentiation of visceral endoderm in the mouse embryo. *Genes Dev*. 1998;12:3579-3590. doi: 10.1101/gad.12.22.3579
8. Tian Y, Yuan L, Goss AM, Wang T, Yang J, Lepore JJ, Zhou D, Schwartz RJ, Patel V, Cohen ED, Morrisey EE. Characterization and in vivo pharmacological rescue of a Wnt2-Gata6 pathway required for cardiac inflow tract development. *Dev Cell*. 2010;18:275-287. doi: 10.1016/j.devcel.2010.01.008
9. van Berlo JH, Elrod JW, van den Hoogenhof MM, York AJ, Aronow BJ, Duncan SA, Molkentin JD. The transcription factor GATA-6 regulates pathological cardiac hypertrophy. *Circ Res*. 2010;107:1032-1040. doi: 10.1161/CIRCRESAHA.110.220764
10. Gharibeh L, Komati H, Bosse Y, Boodhwani M, Heydarpour M, Fortier M, Hassanzadeh R, Ngu J, Mathieu P, Body S, et al. GATA6 Regulates Aortic Valve Remodeling, and Its Haploinsufficiency Leads to Right-Left Type Bicuspid Aortic Valve. *Circulation*. 2018;138:1025-1038. doi: 10.1161/CIRCULATIONAHA.117.029506
11. Gharibeh L, Yamak A, Whitcomb J, Lu A, Joyal M, Komati H, Liang W, Fiset C, Nemer M. GATA6 is a regulator of sinus node development and heart rhythm. *Proc Natl Acad Sci U S A*. 2021;118. doi: 10.1073/pnas.2007322118
12. Wang J, Luo XJ, Xin YF, Liu Y, Liu ZM, Wang Q, Li RG, Fang WY, Wang XZ, Yang YQ. Novel GATA6 mutations associated with congenital ventricular septal defect or tetralogy of fallot. *DNA Cell Biol*. 2012;31:1610-1617. doi: 10.1089/dna.2012.1814

13. Zhang E, Hong N, Chen S, Fu Q, Li F, Yu Y, Sun K. Targeted sequencing identifies novel GATA6 variants in a large cohort of patients with conotruncal heart defects. *Gene*. 2018;641:341-348. doi: 10.1016/j.gene.2017.10.083
14. Gong M, Simaite D, Kuhnen P, Heldmann M, Spagnoli F, Blankenstein O, Hubner N, Hussain K, Raile K. Two novel GATA6 mutations cause childhood-onset diabetes mellitus, pancreas malformation and congenital heart disease. *Horm Res Paediatr*. 2013;79:250-256. doi: 10.1159/000348844
15. Yu L, Bennett JT, Wynn J, Carvill GL, Cheung YH, Shen Y, Mychaliska GB, Azarow KS, Crombleholme TM, Chung DH, et al. Whole exome sequencing identifies de novo mutations in GATA6 associated with congenital diaphragmatic hernia. *J Med Genet*. 2014;51:197-202. doi: 10.1136/jmedgenet-2013-101989
16. Fahed AC, Gelb BD, Seidman JG, Seidman CE. Genetics of congenital heart disease: the glass half empty. *Circ Res*. 2013;112:707-720. doi: 10.1161/CIRCRESAHA.112.300853
17. Seidman JG, Seidman C. Transcription factor haploinsufficiency: when half a loaf is not enough. *J Clin Invest*. 2002;109:451-455. doi: 10.1172/JCI15043
18. Mummery CL, Zhang J, Ng ES, Elliott DA, Elefanty AG, Kamp TJ. Differentiation of human embryonic stem cells and induced pluripotent stem cells to cardiomyocytes: a methods overview. *Circ Res*. 2012;111:344-358. doi: 10.1161/CIRCRESAHA.110.227512
19. Sharma A, Wasson LK, Willcox JA, Morton SU, Gorham JM, DeLaughter DM, Neyazi M, Schmid M, Agarwal R, Jang MY, et al. GATA6 mutations in hiPSCs inform mechanisms for maldevelopment of the heart, pancreas, and diaphragm. *Elife*. 2020;9. doi: 10.7554/eLife.53278
20. Shi ZD, Lee K, Yang D, Amin S, Verma N, Li QV, Zhu Z, Soh CL, Kumar R, Evans T, et al. Genome Editing in hPSCs Reveals GATA6 Haploinsufficiency and a Genetic Interaction with GATA4 in Human Pancreatic Development. *Cell Stem Cell*. 2017;20:675-688 e676. doi: 10.1016/j.stem.2017.01.001
21. Heslop JA, Pournasr B, Liu JT, Duncan SA. GATA6 defines endoderm fate by controlling chromatin accessibility during differentiation of human-induced pluripotent stem cells. *Cell Rep*. 2021;35:109145. doi: 10.1016/j.celrep.2021.109145
22. Chia CY, Madrigal P, Denil S, Martinez I, Garcia-Bernardo J, El-Khairi R, Chhatriwala M, Shepherd MH, Hattersley AT, Dunn NR, Vallier L. GATA6 Cooperates with EOMES/SMAD2/3 to Deploy the Gene Regulatory Network Governing Human Definitive Endoderm and Pancreas Formation. *Stem Cell Reports*. 2019;12:57-70. doi: 10.1016/j.stemcr.2018.12.003
23. Tiyaboonchai A, Cardenas-Diaz FL, Ying L, Maguire JA, Sim X, Jobaliya C, Gagne AL, Kishore S, Stanescu DE, Hughes N, et al. GATA6 Plays an Important Role in the Induction of Human Definitive Endoderm, Development of the Pancreas, and Functionality of Pancreatic beta Cells. *Stem Cell Reports*. 2017;8:589-604. doi: 10.1016/j.stemcr.2016.12.026
24. Ivanovitch K, Soro-Barrio P, Chakravarty P, Jones RA, Bell DM, Mousavy Gharavy SN, Stamataki D, Delile J, Smith JC, Briscoe J. Ventricular, atrial, and outflow tract heart progenitors arise from spatially and molecularly distinct regions of the primitive streak. *PLoS Biol*. 2021;19:e3001200. doi: 10.1371/journal.pbio.3001200

25. Funa NS, Schachter KA, Lerdrup M, Ekberg J, Hess K, Dietrich N, Honore C, Hansen K, Semb H. beta-Catenin Regulates Primitive Streak Induction through Collaborative Interactions with SMAD2/SMAD3 and OCT4. *Cell Stem Cell*. 2015;16:639-652. doi: 10.1016/j.stem.2015.03.008
26. Dubois NC, Craft AM, Sharma P, Elliott DA, Stanley EG, Elefanty AG, Gramolini A, Keller G. SIRPA is a specific cell-surface marker for isolating cardiomyocytes derived from human pluripotent stem cells. *Nat Biotechnol*. 2011;29:1011-1018. doi: 10.1038/nbt.2005
27. Kattman SJ, Witty AD, Gagliardi M, Dubois NC, Niapour M, Hotta A, Ellis J, Keller G. Stage-specific optimization of activin/nodal and BMP signaling promotes cardiac differentiation of mouse and human pluripotent stem cell lines. *Cell Stem Cell*. 2011;8:228-240. doi: 10.1016/j.stem.2010.12.008
28. Gonzalez F, Zhu Z, Shi ZD, Lelli K, Verma N, Li QV, Huangfu D. An iCRISPR platform for rapid, multiplexable, and inducible genome editing in human pluripotent stem cells. *Cell Stem Cell*. 2014;15:215-226. doi: 10.1016/j.stem.2014.05.018
29. Lian X, Hsiao C, Wilson G, Zhu K, Hazeltine LB, Azarin SM, Raval KK, Zhang J, Kamp TJ, Palecek SP. Robust cardiomyocyte differentiation from human pluripotent stem cells via temporal modulation of canonical Wnt signaling. *Proc Natl Acad Sci U S A*. 2012;109:E1848-1857. doi: 10.1073/pnas.1200250109
30. Perl E, Waxman JS. Reiterative Mechanisms of Retinoic Acid Signaling during Vertebrate Heart Development. *J Dev Biol*. 2019;7. doi: 10.3390/jdb7020011
31. Takeda M, Kanki Y, Masumoto H, Funakoshi S, Hatani T, Fukushima H, Izumi-Taguchi A, Matsui Y, Shimamura T, Yoshida Y, Yamashita JK. Identification of Cardiomyocyte-Fated Progenitors from Human-Induced Pluripotent Stem Cells Marked with CD82. *Cell Rep*. 2018;22:546-556. doi: 10.1016/j.celrep.2017.12.057
32. Miquerol L, Kelly RG. Organogenesis of the vertebrate heart. *Wiley Interdiscip Rev Dev Biol*. 2013;2:17-29. doi: 10.1002/wdev.68
33. Gassmann M, Casagranda F, Orioli D, Simon H, Lai C, Klein R, Lemke G. Aberrant neural and cardiac development in mice lacking the ErbB4 neuregulin receptor. *Nature*. 1995;378:390-394. doi: 10.1038/378390a0
34. Loh KM, Chen A, Koh PW, Deng TZ, Sinha R, Tsai JM, Barkal AA, Shen KY, Jain R, Morganti RM, et al. Mapping the Pairwise Choices Leading from Pluripotency to Human Bone, Heart, and Other Mesoderm Cell Types. *Cell*. 2016;166:451-467. doi: 10.1016/j.cell.2016.06.011
35. Prummel KD, Nieuwenhuize S, Mosimann C. The lateral plate mesoderm. *Development*. 2020;147. doi: 10.1242/dev.175059
36. Kimelman D, Griffin KJ. Vertebrate mesendoderm induction and patterning. *Curr Opin Genet Dev*. 2000;10:350-356. doi: 10.1016/s0959-437x(00)00095-2
37. Koh PW, Sinha R, Barkal AA, Morganti RM, Chen A, Weissman IL, Ang LT, Kundaje A, Loh KM. An atlas of transcriptional, chromatin accessibility, and surface marker changes in human mesoderm development. *Sci Data*. 2016;3:160109. doi: 10.1038/sdata.2016.109

38. Tada S, Era T, Furusawa C, Sakurai H, Nishikawa S, Kinoshita M, Nakao K, Chiba T, Nishikawa S. Characterization of mesendoderm: a diverging point of the definitive endoderm and mesoderm in embryonic stem cell differentiation culture. *Development*. 2005;132:4363-4374. doi: 10.1242/dev.02005
39. Probst S, Sagar, Tosic J, Schwan C, Grun D, Arnold SJ. Spatiotemporal sequence of mesoderm and endoderm lineage segregation during mouse gastrulation. *Development*. 2021;148. doi: 10.1242/dev.193789
40. Heslop JA, Pournasr B, Duncan SA. Chromatin remodeling is restricted by transient GATA6 binding during iPSC differentiation to definitive endoderm. *iScience*. 2022;25:104300. doi: 10.1016/j.isci.2022.104300
41. Tosic J, Kim GJ, Pavlovic M, Schroder CM, Mersiowsky SL, Barg M, Hofherr A, Probst S, Kottgen M, Hein L, Arnold SJ. Eomes and Brachyury control pluripotency exit and germ-layer segregation by changing the chromatin state. *Nat Cell Biol*. 2019;21:1518-1531. doi: 10.1038/s41556-019-0423-1
42. Sulahian R, Casey F, Shen J, Qian ZR, Shin H, Ogino S, Weir BA, Vazquez F, Liu XS, Hahn WC, et al. An integrative analysis reveals functional targets of GATA6 transcriptional regulation in gastric cancer. *Oncogene*. 2014;33:5637-5648. doi: 10.1038/onc.2013.517
43. Fisher JB, Pulakanti K, Rao S, Duncan SA. GATA6 is essential for endoderm formation from human pluripotent stem cells. *Biol Open*. 2017;6:1084-1095. doi: 10.1242/bio.026120
44. Costello I, Nowotschin S, Sun X, Mould AW, Hadjantonakis AK, Bikoff EK, Robertson EJ. Lhx1 functions together with Otx2, Foxa2, and Ldb1 to govern anterior mesendoderm, node, and midline development. *Genes Dev*. 2015;29:2108-2122. doi: 10.1101/gad.268979.115
45. Consortium EP, Moore JE, Purcaro MJ, Pratt HE, Epstein CB, Shoresh N, Adrian J, Kawli T, Davis CA, Dobin A, et al. Expanded encyclopaedias of DNA elements in the human and mouse genomes. *Nature*. 2020;583:699-710. doi: 10.1038/s41586-020-2493-4
46. Teo AK, Arnold SJ, Trotter MW, Brown S, Ang LT, Chng Z, Robertson EJ, Dunn NR, Vallier L. Pluripotency factors regulate definitive endoderm specification through eomesodermin. *Genes Dev*. 2011;25:238-250. doi: 10.1101/gad.607311
47. Jha R, Singh M, Wu Q, Gentillon C, Preininger MK, Xu C. Downregulation of LGR5 Expression Inhibits Cardiomyocyte Differentiation and Potentiates Endothelial Differentiation from Human Pluripotent Stem Cells. *Stem Cell Reports*. 2017;9:513-527. doi: 10.1016/j.stemcr.2017.07.006
48. Vincent SD, Mayeuf-Louchart A, Watanabe Y, Brzezinski JAt, Miyagawa-Tomita S, Kelly RG, Buckingham M. Prdm1 functions in the mesoderm of the second heart field, where it interacts genetically with Tbx1, during outflow tract morphogenesis in the mouse embryo. *Hum Mol Genet*. 2014;23:5087-5101. doi: 10.1093/hmg/ddu232
49. Mittal P, Roberts CWM. The SWI/SNF complex in cancer - biology, biomarkers and therapy. *Nat Rev Clin Oncol*. 2020;17:435-448. doi: 10.1038/s41571-020-0357-3

50. Millard CJ, Varma N, Saleh A, Morris K, Watson PJ, Bottrill AR, Fairall L, Smith CJ, Schwabe JW. The structure of the core NuRD repression complex provides insights into its interaction with chromatin. *Elife*. 2016;5:e13941. doi: 10.7554/eLife.13941
51. Sun Y, Kolligs FT, Hottiger MO, Mosavin R, Fearon ER, Nabel GJ. Regulation of beta -catenin transformation by the p300 transcriptional coactivator. *Proc Natl Acad Sci U S A*. 2000;97:12613-12618. doi: 10.1073/pnas.220158597
52. Valenta T, Lukas J, Korinek V. HMG box transcription factor TCF-4's interaction with CtBP1 controls the expression of the Wnt target Axin2/Conductin in human embryonic kidney cells. *Nucleic Acids Res*. 2003;31:2369-2380. doi: 10.1093/nar/gkg346
53. Cuilliere-Dartigues P, El-Bchiri J, Krimi A, Buhard O, Fontanges P, Flejou JF, Hamelin R, Duval A. TCF-4 isoforms absent in TCF-4 mutated MSI-H colorectal cancer cells colocalize with nuclear CtBP and repress TCF-4-mediated transcription. *Oncogene*. 2006;25:4441-4448. doi: 10.1038/sj.onc.1209471
54. Brantjes H, Roose J, van De Wetering M, Clevers H. All Tcf HMG box transcription factors interact with Groucho-related co-repressors. *Nucleic Acids Res*. 2001;29:1410-1419. doi: 10.1093/nar/29.7.1410
55. Stavish D, Boiers C, Price C, Frith TJR, Halliwell J, Saldana-Guerrero I, Wray J, Brown J, Carr J, James C, et al. Generation and trapping of a mesoderm biased state of human pluripotency. *Nat Commun*. 2020;11:4989. doi: 10.1038/s41467-020-18727-8
56. Ueno S, Weidinger G, Osugi T, Kohn AD, Golob JL, Pabon L, Reinecke H, Moon RT, Murry CE. Biphasic role for Wnt/beta-catenin signaling in cardiac specification in zebrafish and embryonic stem cells. *Proc Natl Acad Sci U S A*. 2007;104:9685-9690. doi: 10.1073/pnas.0702859104
57. de Lau W, Peng WC, Gros P, Clevers H. The R-spondin/Lgr5/Rnf43 module: regulator of Wnt signal strength. *Genes Dev*. 2014;28:305-316. doi: 10.1101/gad.235473.113
58. Sahara M, Santoro F, Sohlmer J, Zhou C, Witman N, Leung CY, Mononen M, Bylund K, Gruber P, Chien KR. Population and Single-Cell Analysis of Human Cardiogenesis Reveals Unique LGR5 Ventricular Progenitors in Embryonic Outflow Tract. *Dev Cell*. 2019;48:475-490 e477. doi: 10.1016/j.devcel.2019.01.005
59. Lei I, Gao X, Sham MH, Wang Z. SWI/SNF protein component BAF250a regulates cardiac progenitor cell differentiation by modulating chromatin accessibility during second heart field development. *J Biol Chem*. 2012;287:24255-24262. doi: 10.1074/jbc.M112.365080
60. Hota SK, Johnson JR, Verschueren E, Thomas R, Blotnick AM, Zhu Y, Sun X, Pennacchio LA, Krogan NJ, Bruneau BG. Dynamic BAF chromatin remodeling complex subunit inclusion promotes temporally distinct gene expression programs in cardiogenesis. *Development*. 2019;146. doi: 10.1242/dev.174086
61. Hota SK, Rao KS, Blair AP, Khalilimeybodi A, Hu KM, Thomas R, So K, Kameswaran V, Xu J, Polacco BJ, et al. Brahma safeguards canalization of cardiac mesoderm differentiation. *Nature*. 2022;602:129-134. doi: 10.1038/s41586-021-04336-y

62. Herchenrother A, Gossen S, Friedrich T, Reim A, Daus N, Diegmuller F, Leers J, Sani HM, Gerstner S, Schwarz L, et al. The H2A.Z and NuRD associated protein HMG20A controls early head and heart developmental transcription programs. *Nat Commun*. 2023;14:472. doi: 10.1038/s41467-023-36114-x
63. Shi W, Wasson LK, Dorr KM, Robbe ZL, Wilczewski CM, Hepperla AJ, Davis IJ, Seidman CE, Seidman JG, Conlon FL. CHD4 and SMYD1 repress common transcriptional programs in the developing heart. *Development*. 2024;151. doi: 10.1242/dev.202505
64. Takaku M, Grimm SA, Shimbo T, Perera L, Menafra R, Stunnenberg HG, Archer TK, Machida S, Kurumizaka H, Wade PA. GATA3-dependent cellular reprogramming requires activation-domain dependent recruitment of a chromatin remodeler. *Genome Biol*. 2016;17:36. doi: 10.1186/s13059-016-0897-0
65. Lickert H, Takeuchi JK, Von Both I, Walls JR, McAuliffe F, Adamson SL, Henkelman RM, Wrana JL, Rossant J, Bruneau BG. Baf60c is essential for function of BAF chromatin remodelling complexes in heart development. *Nature*. 2004;432:107-112. doi: 10.1038/nature03071
66. Wolf BK, Zhao Y, McCray A, Hawk WH, Deary LT, Sugiarto NW, LaCroix IS, Gerber SA, Cheng C, Wang X. Cooperation of chromatin remodeling SWI/SNF complex and pioneer factor AP-1 shapes 3D enhancer landscapes. *Nat Struct Mol Biol*. 2023;30:10-21. doi: 10.1038/s41594-022-00880-x
67. Chea S, Kreger J, Lopez-Burks ME, MacLean AL, Lander AD, Calof AL. Gastrulation-stage gene expression in Nipbl(+/-) mouse embryos foreshadows the development of syndromic birth defects. *Sci Adv*. 2024;10:eadl4239. doi: 10.1126/sciadv.adl4239
68. Yang D, Gomez-Garcia J, Funakoshi S, Tran T, Fernandes I, Bader GD, Laflamme MA, Keller GM. Modeling human multi-lineage heart field development with pluripotent stem cells. *Cell Stem Cell*. 2022;29:1382-1401 e1388. doi: 10.1016/j.stem.2022.08.007
69. Murry CE, Keller G. Differentiation of embryonic stem cells to clinically relevant populations: lessons from embryonic development. *Cell*. 2008;132:661-680. doi: 10.1016/j.cell.2008.02.008
70. Ran FA, Hsu PD, Wright J, Agarwala V, Scott DA, Zhang F. Genome engineering using the CRISPR-Cas9 system. *Nat Protoc*. 2013;8:2281-2308. doi: 10.1038/nprot.2013.143
71. Yamaguchi T, Hamanaka S, Kamiya A, Okabe M, Kawarai M, Wakiyama Y, Umino A, Hayama T, Sato H, Lee YS, et al. Development of an all-in-one inducible lentiviral vector for gene specific analysis of reprogramming. *PLoS One*. 2012;7:e41007. doi: 10.1371/journal.pone.0041007
72. Lan Y, Banks KM, Pan H, Verma N, Dixon GR, Zhou T, Ding B, Elemento O, Chen S, Huangfu D, Evans T. Stage-specific regulation of DNA methylation by TET enzymes during human cardiac differentiation. *Cell Rep*. 2021;37:110095. doi: 10.1016/j.celrep.2021.110095
73. Anelli V, Villefranc JA, Chhangawala S, Martinez-McFaline R, Riva E, Nguyen A, Verma A, Bareja R, Chen Z, Scognamiglio T, et al. Oncogenic BRAF disrupts thyroid morphogenesis and function via twist expression. *Elife*. 2017;6. doi: 10.7554/eLife.20728

74. Dobin A, Davis CA, Schlesinger F, Drenkow J, Zaleski C, Jha S, Batut P, Chaisson M, Gingeras TR. STAR: ultrafast universal RNA-seq aligner. *Bioinformatics*. 2013;29:15-21. doi: 10.1093/bioinformatics/bts635
75. Trapnell C, Hendrickson DG, Sauvageau M, Goff L, Rinn JL, Pachter L. Differential analysis of gene regulation at transcript resolution with RNA-seq. *Nat Biotechnol*. 2013;31:46-53. doi: 10.1038/nbt.2450
76. Trapnell C, Williams BA, Pertea G, Mortazavi A, Kwan G, van Baren MJ, Salzberg SL, Wold BJ, Pachter L. Transcript assembly and quantification by RNA-Seq reveals unannotated transcripts and isoform switching during cell differentiation. *Nat Biotechnol*. 2010;28:511-515. doi: 10.1038/nbt.1621
77. Anders S, Pyl PT, Huber W. HTSeq--a Python framework to work with high-throughput sequencing data. *Bioinformatics*. 2015;31:166-169. doi: 10.1093/bioinformatics/btu638
78. Love MI, Huber W, Anders S. Moderated estimation of fold change and dispersion for RNA-seq data with DESeq2. *Genome Biol*. 2014;15:550. doi: 10.1186/s13059-014-0550-8
79. Subramanian A, Tamayo P, Mootha VK, Mukherjee S, Ebert BL, Gillette MA, Paulovich A, Pomeroy SL, Golub TR, Lander ES, Mesirov JP. Gene set enrichment analysis: a knowledge-based approach for interpreting genome-wide expression profiles. *Proc Natl Acad Sci U S A*. 2005;102:15545-15550. doi: 10.1073/pnas.0506580102
80. Castanza AS, Recla JM, Eby D, Thorvaldsdottir H, Bult CJ, Mesirov JP. Extending support for mouse data in the Molecular Signatures Database (MSigDB). *Nat Methods*. 2023;20:1619-1620. doi: 10.1038/s41592-023-02014-7
81. Huang da W, Sherman BT, Lempicki RA. Systematic and integrative analysis of large gene lists using DAVID bioinformatics resources. *Nat Protoc*. 2009;4:44-57. doi: 10.1038/nprot.2008.211
82. Sherman BT, Hao M, Qiu J, Jiao X, Baseler MW, Lane HC, Imamichi T, Chang W. DAVID: a web server for functional enrichment analysis and functional annotation of gene lists (2021 update). *Nucleic Acids Res*. 2022;50:W216-W221. doi: 10.1093/nar/gkac194
83. Tang D, Chen M, Huang X, Zhang G, Zeng L, Zhang G, Wu S, Wang Y. SRplot: A free online platform for data visualization and graphing. *PLoS One*. 2023;18:e0294236. doi: 10.1371/journal.pone.0294236
84. Mohammed H, Taylor C, Brown GD, Papachristou EK, Carroll JS, D'Santos CS. Rapid immunoprecipitation mass spectrometry of endogenous proteins (RIME) for analysis of chromatin complexes. *Nat Protoc*. 2016;11:316-326. doi: 10.1038/nprot.2016.020

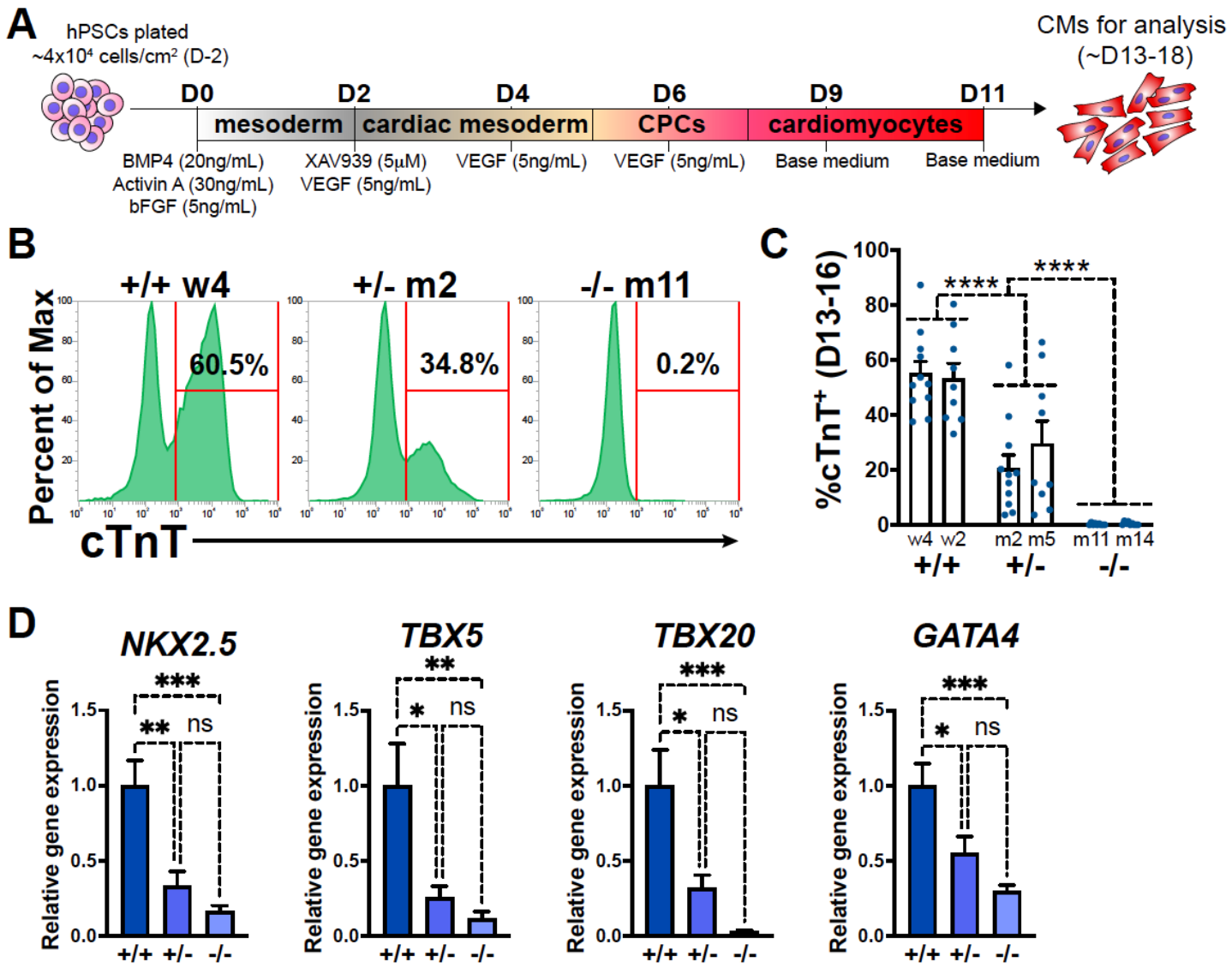

Figure 1. GATA6 loss-of-function inhibits CM and CPC development. (**A**) Schematic for *in vitro* CM directed differentiation cytokine-based protocol. Color gradients represent relative developmental stages (white: pluripotent, grey: mesoderm, yellow: cardiac mesoderm, pink: CPCs, and red: CMs). (**B**) Representative flow cytometry plots for cTnT^{+} CMs at day 14 of cardiac differentiation for *GATA6*$^{+/+}$, *GATA6*$^{+/-}$, and *GATA6*$^{-/-}$ hESCs. (**C**) %cTnT^{+} CMs quantified by flow cytometry between days 13 and 16 (dots indicate independent biological replicates). Significance indicated as ****P<0.0001 by two-way ANOVA with Tukey's multiple comparison test by genotype. There was no significant difference between clones of the same genotype when two-way ANOVA and Tukey's multiple comparison test was performed for all six sample groups. (**D**) Day 6 RT-qPCR for the CPC markers indicated normalized to *GATA6*$^{+/+}$ (n=6). Data represents the mean ± SEM, significance indicated as *p<0.05, **p<0.01, ***p<0.001, ns indicates not significant as determined by one-way ANOVA and Tukey's multiple comparisons test.

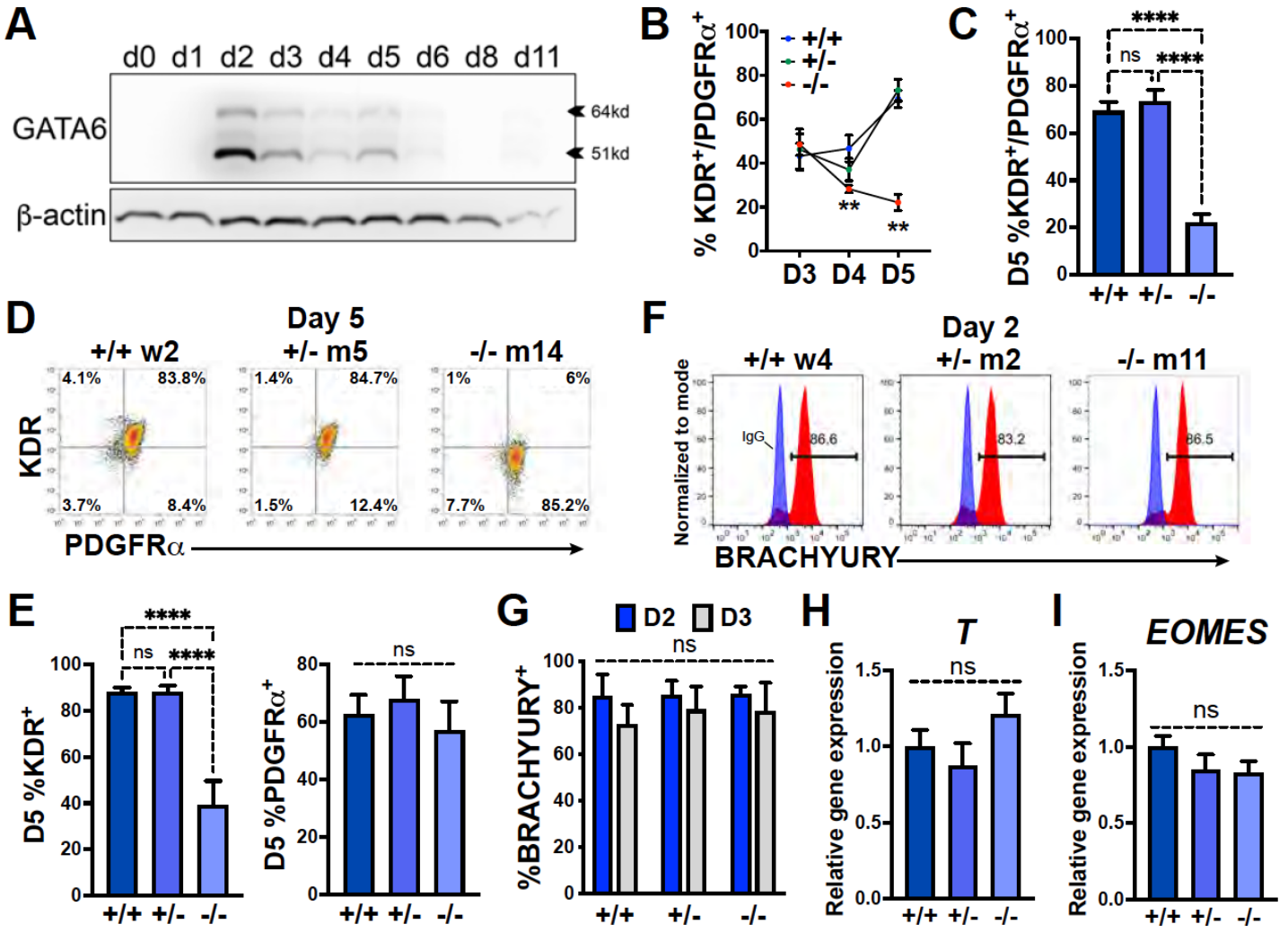

Figure 2. GATA6 is required for cardiac mesoderm development. (**A**) Western blot time course using protein lysates from *GATA6*$^{+/+}$ hESCs probed for GATA6 with β-actin used as a loading control. (**B**) Flow cytometry quantification for % KDR and PDGFRα double-positive (%K$^+$P$^+$) cells from days 3 to 5 of cardiac differentiation of *GATA6*$^{+/+}$, *GATA6*$^{+/-}$, or *GATA6*$^{-/-}$ hESCs (n≥4). Asterisks indicate statistical significance comparing *GATA6*$^{-/-}$ and WT on days 4 or 5 of cardiac differentiation. (**C**) Day 5 flow cytometry quantification for %K$^+$P$^+$ cells (n=7). **D**) Representative flow cytometry plots for day 5 %K$^+$P$^+$ cells. (**E**) Day 5 flow cytometry quantification (n=7) for %KDR$^+$ (left) or PDGFRα$^+$ (right). (**F**) Representative flow cytometry plots for day 2 %BRACHYURY$^+$ cells (red) overlaid IgG stained controls (blue). (**G**) Quantification for day 2 or day 3 %BRACHYURY$^+$ cells (n=4). (**H**) RT-qPCR for day 2 *T* expression levels normalized to *GATA6*$^{+/+}$ samples (n=6). (**I**) RT-qPCR for day 2 *EOMES* expression levels normalized to *GATA6*$^{+/+}$ samples (n=6). Data represents the mean ± SEM, with significance indicated as **p<0.01, ****p<0.0001, and ns indicating not significant by two-way ANOVA (B and G) or one-way ANOVA (C, E, H, and I) with Tukey's multiple comparison test.

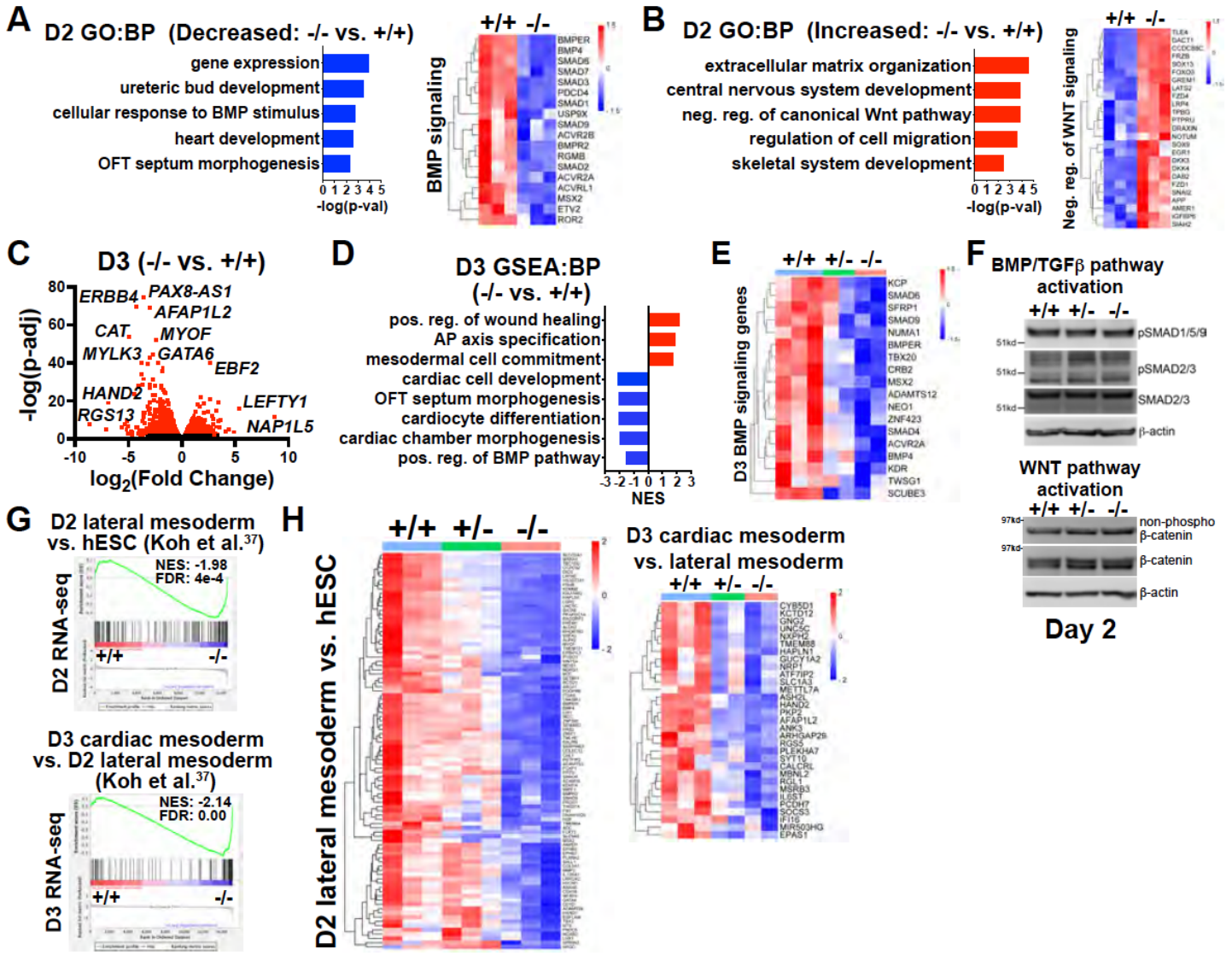

Figure 3. Transcriptome analysis at early mesoderm patterning stages. (**A**) Gene Ontology (GO) analysis for biological process (BP) from decreased differentially expressed genes (dDEGs) identified comparing *GATA6*$^{-/-}$ to WT samples from day 2 RNA-seq data (left). Heatmap for genes related to BMP signaling from day 2 RNA-seq shown on the right. Color gradient on heatmap indicates relative gene expression levels. (**B**) GO analysis (BP) of increased DEGs identified comparing *GATA6*$^{+/-}$ to WT samples from day 2 RNA-seq (left). Heatmap for genes related to negative regulation of canonical WNT pathway from day 2 RNA-seq shown on the right. (**C**) Volcano plot for day 2 *GATA6*$^{-/-}$ sample RNA-seq gene expression data relative to WT controls. Dots represent genes, red indicates p-adj<0.05 and black indicates p-adj>0.05. (**D**) Gene set enrichment analysis (GSEA) (BP) of *GATA6*$^{-/-}$ cells relative to WT controls from day 3 RNA-seq data. NES indicates normalized enrichment score. (**E**) Heatmap for BMP signaling genes from day 3 RNA-seq data. (**F**) Western blots using protein lysates from *GATA6*$^{+/+}$, *GATA6*$^{+/-}$ or *GATA6*$^{-/-}$ cells at day 2 of cardiac differentiation probed with antibodies recognizing phospho-SMAD1/5/9, phospho-SMAD2/3, total SMAD2/3, non-phospho-β-catenin, and total β-catenin with β-actin used as a loading control. (**G**) GSEA analysis of day 2 or day 3 RNA-seq gene expression data (*GATA6*$^{-/-}$ relative to WT) using the day 2 lateral mesoderm (relative to hESC, left) and day 3 cardiac mesoderm (relative

to day 2 lateral mesoderm, right) during hESC cardiac differentiation datasets from Koh et al. (Ref. 37) NES indicates normalized enrichment score; FDR indicates false discovery rate. **H**) Heatmaps from RNA-seq day 2 (left) or day 3 (right) data using core enrichment genes identified in (G) for lateral mesoderm (relative to hESCs) and cardiac mesoderm (relative to lateral mesoderm).

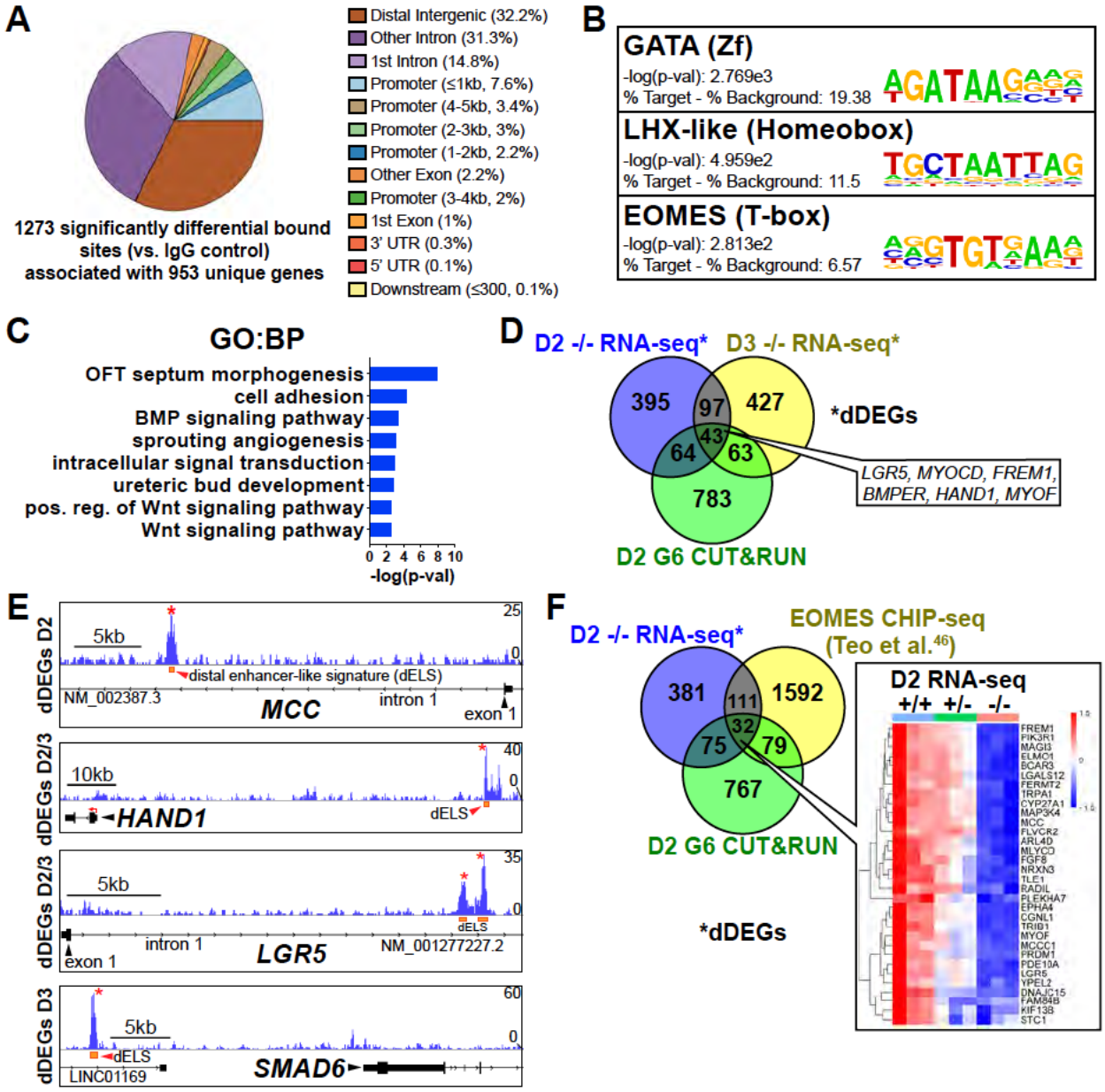

Figure 4: GATA6 CUT&RUN analysis during early mesoderm patterning. (**A**) Genomic distribution for significant GATA6 binding peaks identified by GATA6 CUT&RUN at day 2 of cardiac differentiation (n=3). (**B**) Transcription factor motif enrichment at GATA6 bound loci. (**C**) GO (BP) analysis of the gene list associated with significant GATA6 binding peaks. (**D**) Venn diagram comparisons for day 2 GATA6 CUT&RUN identified genes (green), day 2 dDEGs (blue) and day 3 dDEGs (yellow) identified by RNA-seq (*GATA6*$^{-/-}$ relative to WT). (**E**) Human genome browser representations of GATA6 CUT&RUN data (blue tracks) aligned to select genes that are dDEGs identified by day 2 or 3 RNA-seq (*GATA6*$^{-/-}$ relative to WT). Orange rectangles represent approximate location for distal enhancer-like signatures (dELS) via the ENCODE Project. Asterisks indicate significant GATA6 binding peaks ($p<0.003$ relative to IgG controls). (**F**) Venn diagram comparisons for day 2 GATA6 CUT&RUN

identified genes (green), day 2 dDEGs (blue, *GATA6*$^{-/-}$ relative to WT) and EOMES-CHIP-seq identified genes at day 2 of hESC-DE differentiation from Teo et al. (Ref. 46) (yellow). Inlayed heatmap indicates *GATA6*$^{+/+}$, *GATA6*$^{+/-}$ and *GATA6*$^{-/-}$ RNA-seq gene expression data at day 2 of cardiac differentiation for the 32 triple-overlap genes.

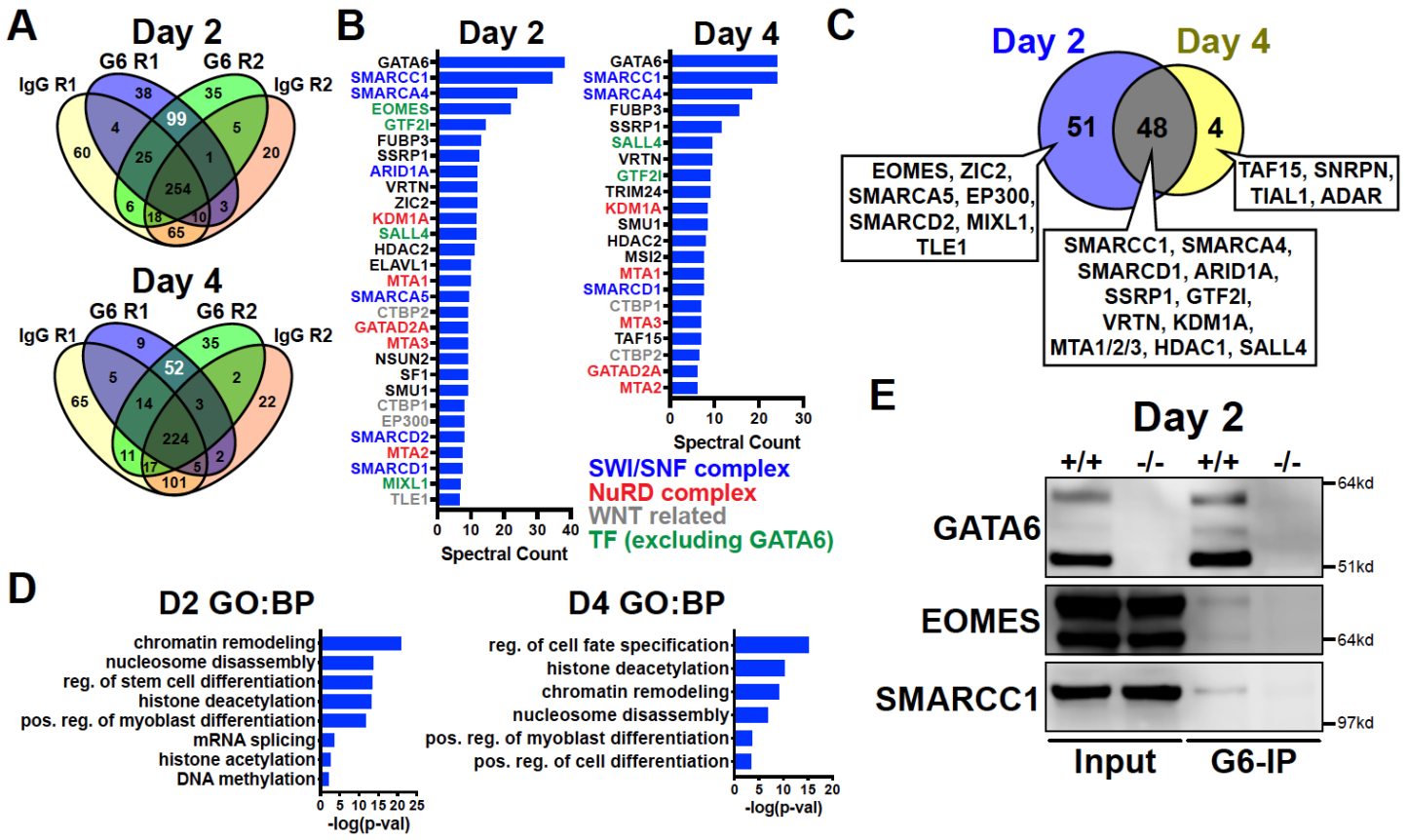

Figure 5. GATA6 interactome analysis during precardiac to cardiac mesoderm patterning stages. (**A**) Venn diagrams showing unique proteins identified by RIME analysis performed on *GATA6*$^{+/+}$ hESCs at day 2 or day 4 of cardiac differentiation. Numbers in white text indicate enriched proteins identified by GATA6-RIME. G6 indicates GATA6, R indicates replicate (n=2). (**B**) Enriched proteins identified by GATA6 RIME (spectral count >5, unique peptides >1). (**C**) Venn diagram comparing day 2 (blue) and day 4 (yellow) GATA6-RIME enriched proteins. (**D**) GO (BP) analysis for GATA6-RIME enriched proteins on days 2 or 4. (**E**) Western blots for GATA6, EOMES, and SMARCC1 performed on GATA6-immunoprecipitated (G6-IP) whole-cell protein lysates from *GATA6*$^{+/+}$ and *GATA6*$^{-/-}$ cells isolated at day 2 of cardiac differentiation. Input indicates whole-cell protein lysate controls.

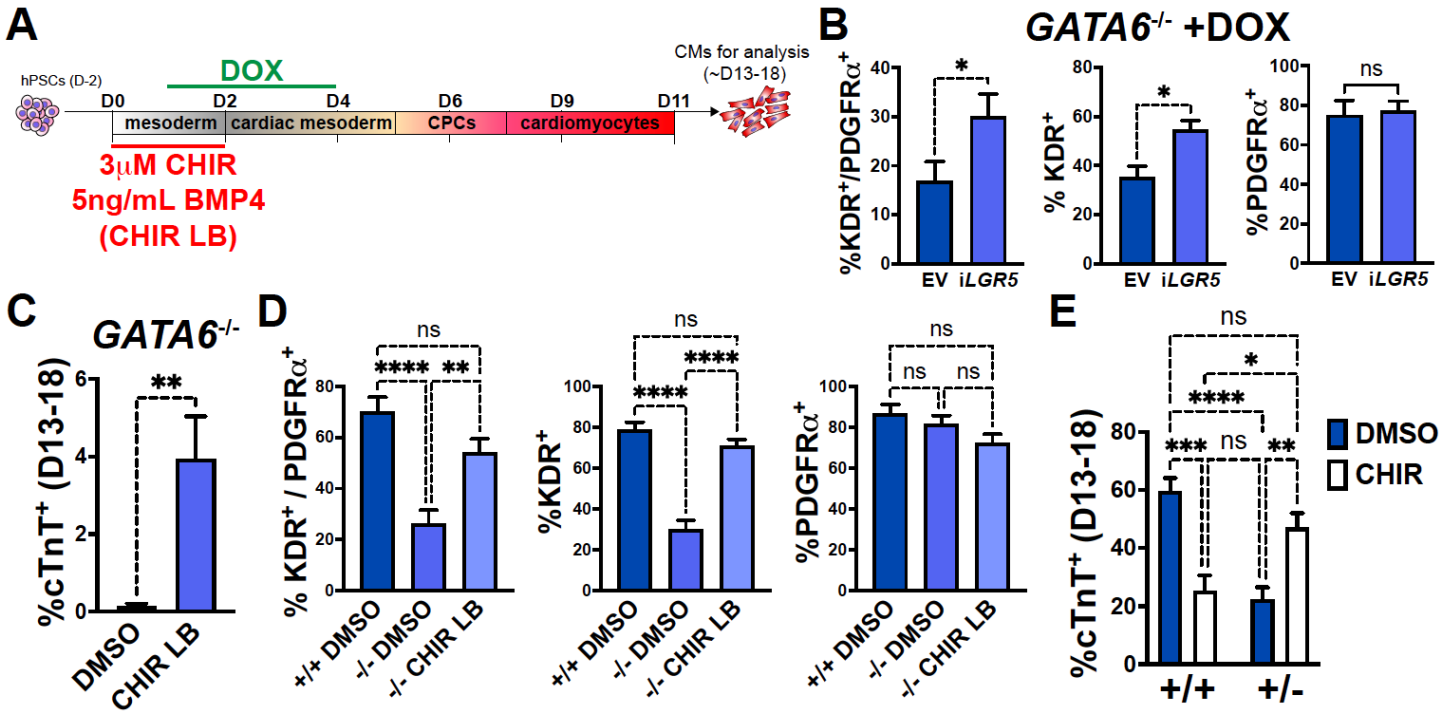

Figure 6. Early manipulation of the WNT and BMP pathways partially rescues the CM defects in GATA6 loss-of-function hESCs. (**A**) Schematic for treatment with DOX (days 1-4), CHIR (3μM, days 0-2), and/or reduced BMP4 (5ng/mL, days 0-2, indicated as "LB") during CM directed differentiation. (**B**) Day 5 flow cytometry quantification for %K^+P^+ double-positive cells, %KDR^+ single-positive cells, or %PDGFRα^+ single-positive cells in *GATA6*$^{-/-}$ hESCs transduced with i*LGR5* or empty vector (EV) (n=5). Significance indicated by *p<0.05 according to a two-tailed paired Student's t-test. (**C**) %$cTnT^+$ CMs from days 13-18 of cardiac differentiation quantified by flow cytometry in *GATA6*$^{-/-}$ cells treated with CHIR LB or vehicle (DMSO) with normal BMP4 concentration treated control (n≥6). (**D**) Flow cytometry at day 5 of cardiac differentiation to quantifiy %K^+P^+ double-positive, %KDR^+ single-positive, or %PDGFRα^+ single-positive cells comparing *GATA6*$^{-/-}$ hESCs treated with CHIR LB with *GATA6*$^{+/+}$ and *GATA6*$^{-/-}$ hESCs controls treated with vehicle and normal BMP4 concentration (n≥8). (**E**) %$cTnT^+$ CMs from days 13-18 of cardiac differentiation quantified by flow cytometry in *GATA6*$^{+/-}$ or WT hESCs treated with CHIR (3μM) or DMSO (n≥7). Data represents the mean ± SEM, significance indicated by **p<0.01, ***p<0.001, ****p<0.0001 by two-tailed Student's t-test (C) and one-way ANOVA (D) or two-way ANOVA (E) with Tukey's multiple comparisons test.

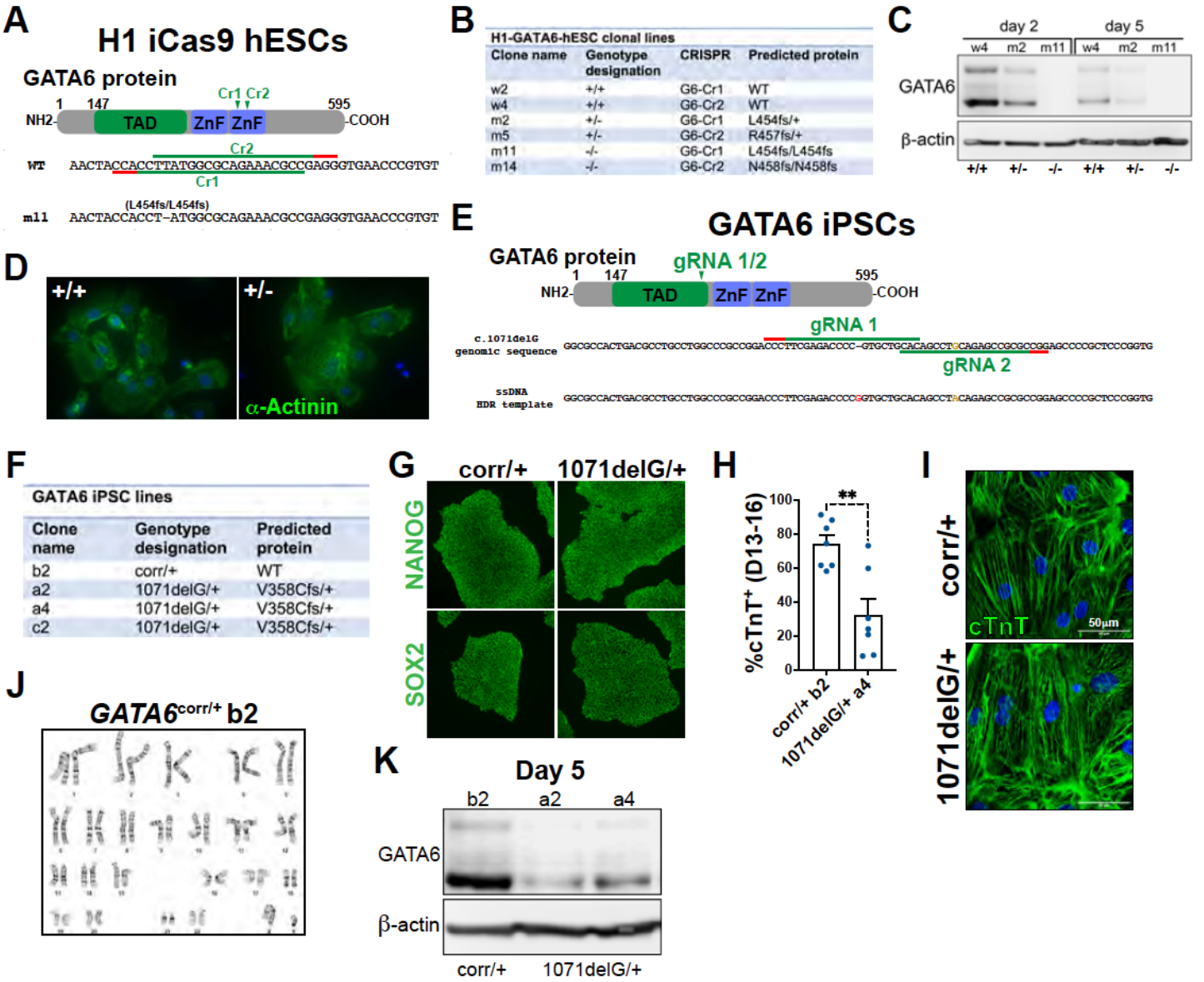

Supplemental Figure 1: CRISPR gene editing and characterization of mutant GATA6 hESC and iPSC lines. (**A**) GATA6 CRISPR targeting scheme using H1 iCas9 hESCs was described in Shi et al. (Ref. 20). Two CRISPR gRNAs were used targeting the C-terminal zinc finger domain (GATA6-Cr1 and Cr2 gRNA target sequence in green, red indicates the PAM). (**B**) Table describing H1-GATA6-hESC clonal lines, genotype designation, and gRNA used in gene editing. Predicted protein describes mutant alleles according to the Human Genome Variation Society (HGVS) guidelines, fs indicates frameshift mutation. (**C**) Western blots from *GATA6*$^{+/+}$, *GATA6*$^{+/-}$, and *GATA6*$^{-/-}$ protein lysates at day 2 or 5 of cardiac differentiation probed for GATA6 with β-actin used as a loading control. (**D**) Immunofluorescence for the sarcomere marker α-Actinin and co-stained with DAPI on day 23 lactate-purified CMs. (**E**) Schematic for CRISPR-based correction of the GATA6 c.1071delG iPSC mutant allele to WT sequence (*GATA6*$^{corr/+}$). A pair of gRNAs flanking the G deletion site were used for targeting with Nickase-Cas9 and a WT repair template to allow for homology directed repair (HDR) of the mutant allele. A single base substitution of G to A (indicated by brown) was used in the WT repair template to induce a silent mutation in the gRNA 2 recognition sequence to prevent additional Cas9 activity after HDR. (**F**) Table describing

the GATA6 iPSC clonal lines. The GATA6 c.1071delG mutant allele is indicated as the protein V358Cfs (according to HGVS guidelines). (**G**) Immunofluorescence for the pluripotency markers NANOG or SOX2 on *GATA6*$^{corr/+}$ or *GATA6*$^{1071delG/+}$ iPSC colonies. (**H**) Flow cytometry quantification for %cTnT^{+} CMs following cardiac directed differentiation for days 13 to 16 of *GATA6*$^{corr/+}$ or *GATA6*$^{1071delG/+}$ iPSCs. Data represents the mean ± SEM, dots represent independent biological replicates. Significance defined as **$p<0.01$ using the two-tailed Student's T-test. (**I**) Immunofluorescence for cTnT and co-stained with DAPI on day 23 lactate-purified iPSC-CMs. (**J**) Representative karyogram for *GATA6*$^{corr/+}$ iPSCs. (**K**) Western blots from *GATA6*$^{corr/+}$ or *GATA6*$^{1071delG/+}$ protein lysates at day 5 of cardiac differentiation probed for GATA6 with β-actin used as a loading control.

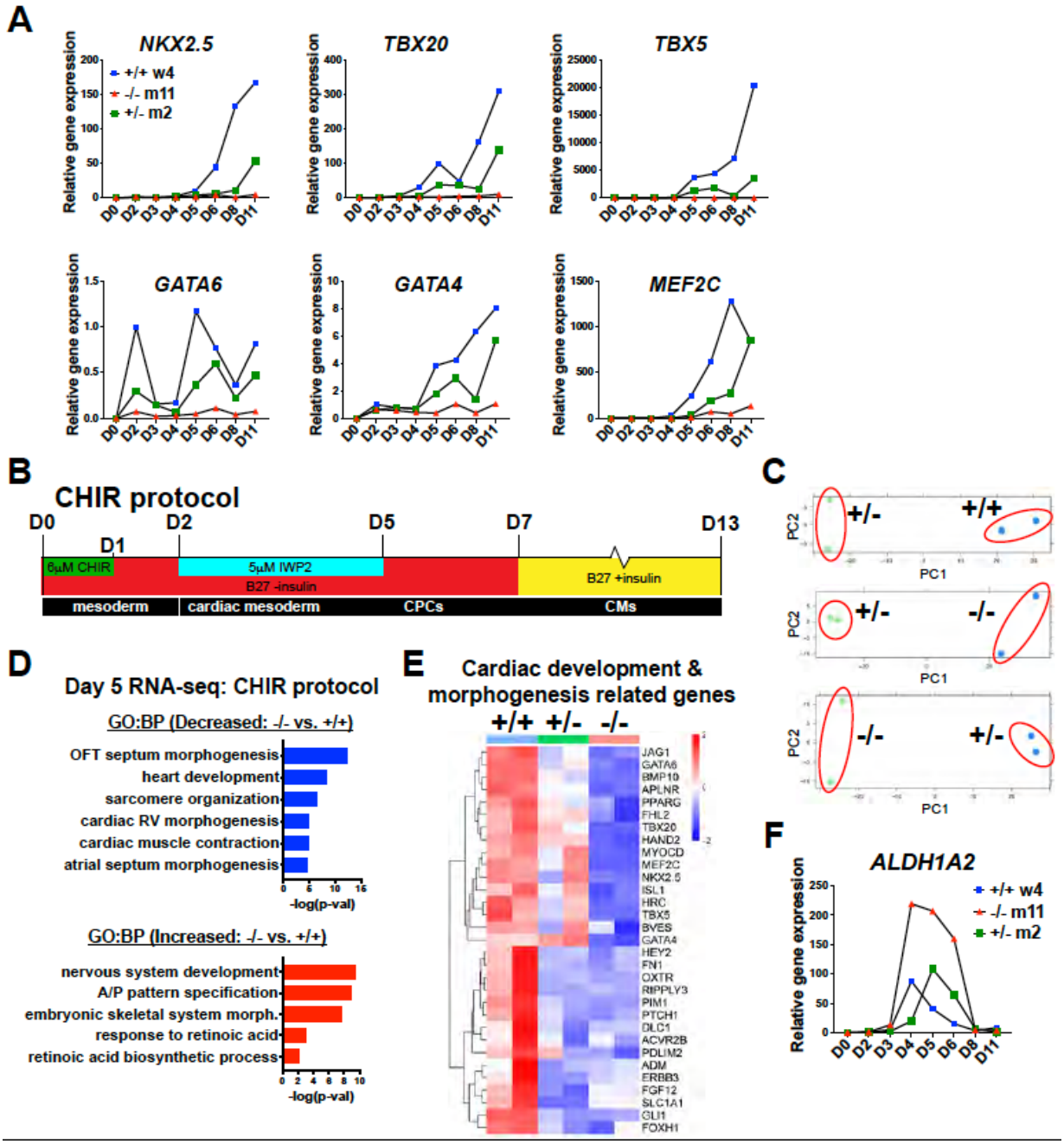

Supplemental Figure 2: CPC marker gene transcriptional analysis of GATA6 WT or mutant hESCs. (**A**) RT-qPCR time course for CPC markers (and *GATA6*) in differentiating *GATA6*$^{+/+}$, *GATA6*$^{+/-}$, and *GATA6*$^{-/-}$ hESCs (normalized to day 2 WT gene expression levels). (**B**) Schematic for *in vitro* CM directed differentiation CHIR protocol. (**C**) Principal component analysis (PCA) for pairwise comparisons of day 5 bulk RNA-seq from *GATA6*$^{+/+}$, *GATA6*$^{+/-}$, and *GATA6*$^{-/-}$ hESCs using the CHIR protocol (n=2). (**D**) Gene ontology (GO) analysis for biological process (BP) using differentially expressed genes (DEGs) from day 5 RNA-seq comparing *GATA6*$^{-/-}$ to WT. (**E**) Heatmap for cardiac development related genes from day 5 RNA-seq. Color gradient indicates relative gene expression level. (**F**) RT-qPCR time course for *ALDH1A2* transcript levels in differentiating *GATA6*$^{+/+}$, *GATA6*$^{+/-}$, and *GATA6*$^{-/-}$ hESCs using the cytokine-based protocol.

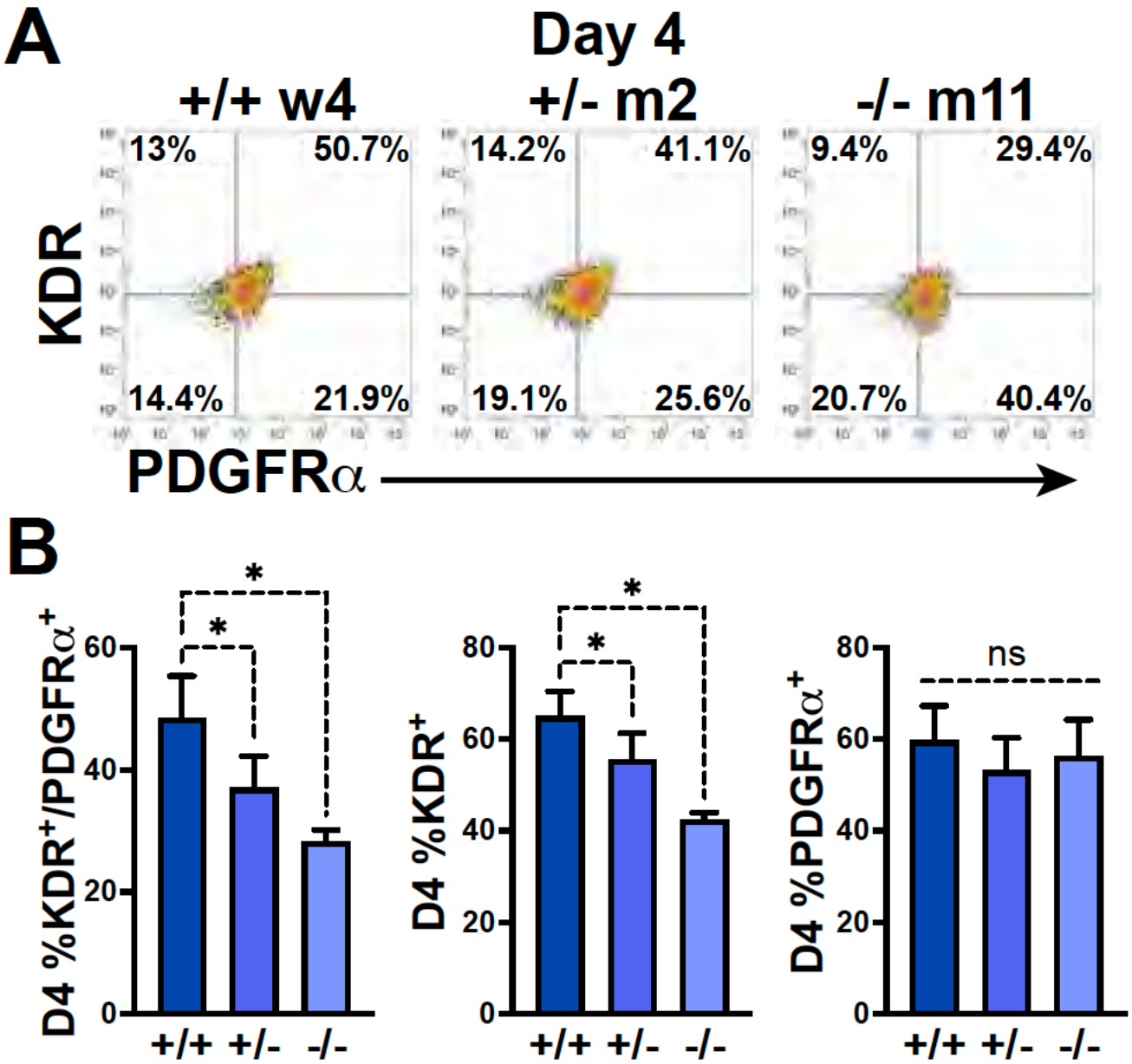

Supplemental Figure 3: KDR and PDGFRα cardiac mesoderm analysis at day 4. (**A**) Representative flow cytometry plots at day 4 of cardiac differentiation analyzing the % KDR and PDGFRα double-positive cells (%K^+P^+) from *GATA6*$^{+/+}$, *GATA6*$^{+/-}$, or *GATA6*$^{-/-}$ hESCs. (**B**) Quantification of day 4 flow cytometry data for %K^+P^+ double-positive, %KDR^+ single positive, or %$PDGFR\alpha^+$ single positive cells (n=6). Data represent the mean ± SEM, with statistical significance indicated as *$p<0.05$ and ns indicating not significant by one-way repeated measures ANOVA with Holm-Šídák's multiple comparison test.

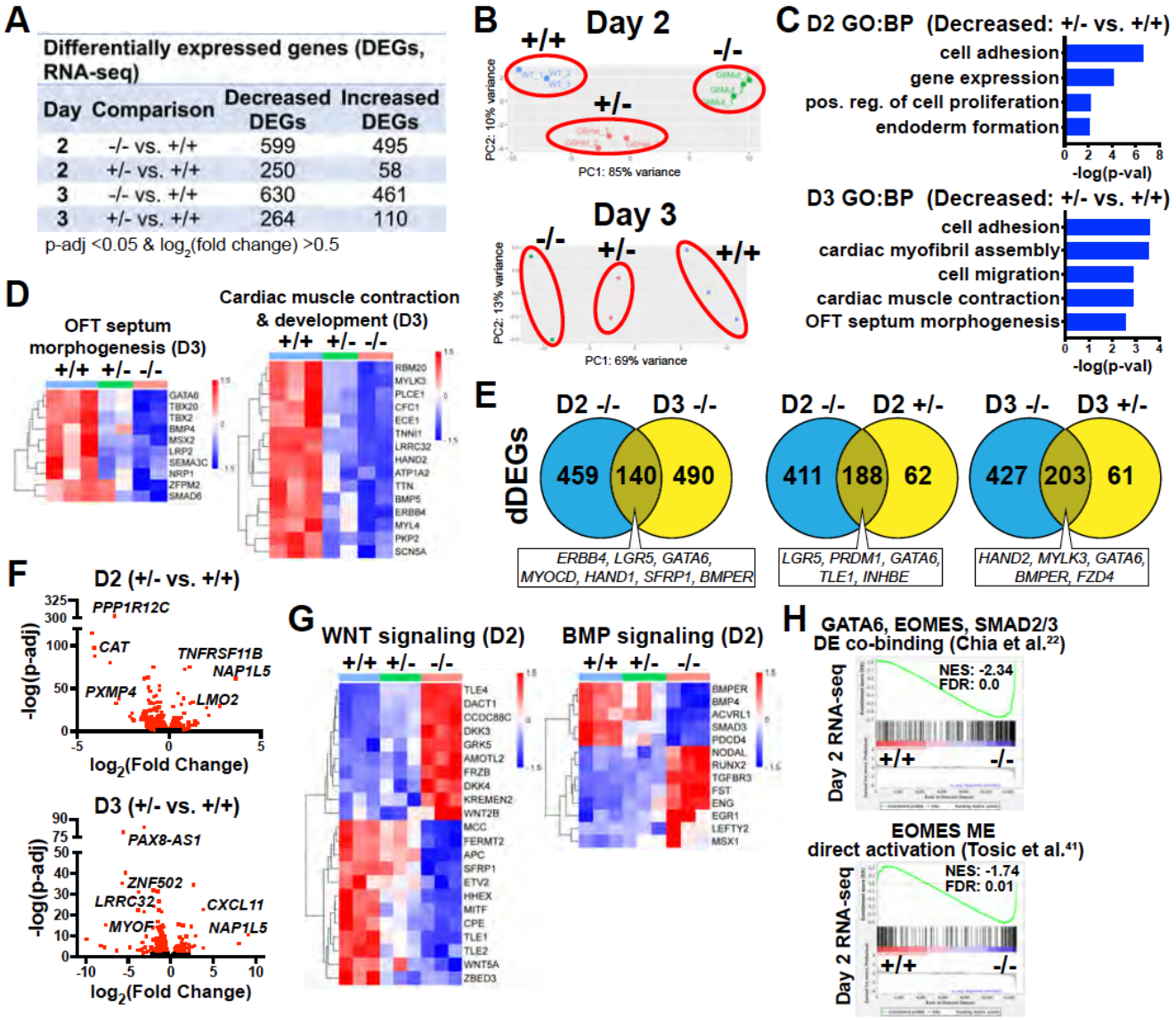

Supplemental Figure 4: RNA-seq analysis following cardiac differentiation at day 2 or day 3. (**A**) Number of DEGs identified when comparing *GATA6*$^{+/-}$ and *GATA6*$^{-/-}$ samples to *GATA6*$^{+/+}$ controls from day 2 and 3 RNA-seq data. **B**) PCA analysis for *GATA6*$^{+/+}$, *GATA6*$^{+/-}$, and *GATA6*$^{-/-}$ profiles from day 2 or day 3 RNA-seq. Data is representative of at least 2 independent biological replicates per sample. (**C**) Day 2 and 3 GO (BP) analysis using dDEGs identified comparing *GATA6*$^{+/-}$ to WT samples. (**D**) Heatmaps for OFT septum morphogenesis and cardiac development related genes from day 3 RNA-seq. Color gradient indicates relative gene expression levels. (**E**) Venn diagram comparisons of dDEGs (relative to WT) identified by day 2 or day 3 RNA-seq of *GATA6*$^{+/-}$ and *GATA6*$^{-/-}$ samples. (**F**) Volcano plots for day 2 or 3 *GATA6*$^{+/-}$ sample RNA-seq gene expression data relative to WT. Dots represent genes, red indicates p-adj<0.05 and black indicates p-adj>0.05. (**G**) Heatmaps for WNT and BMP related genes from day 2 RNA-seq. (**H**) Gene set enrichment analysis (GSEA) analysis of day 2 RNA-seq gene expression data (*GATA6*$^{-/-}$ relative to WT) using the GATA6, EOMES, and SMAD2/3 co-binding during hESC-DE differentiation dataset from Chia et al. (Ref. 22) and EOMES ME direct activation dataset from Tosic et al. (Ref. 41). NES indicates normalized enrichment score; FDR indicates false discovery rate.

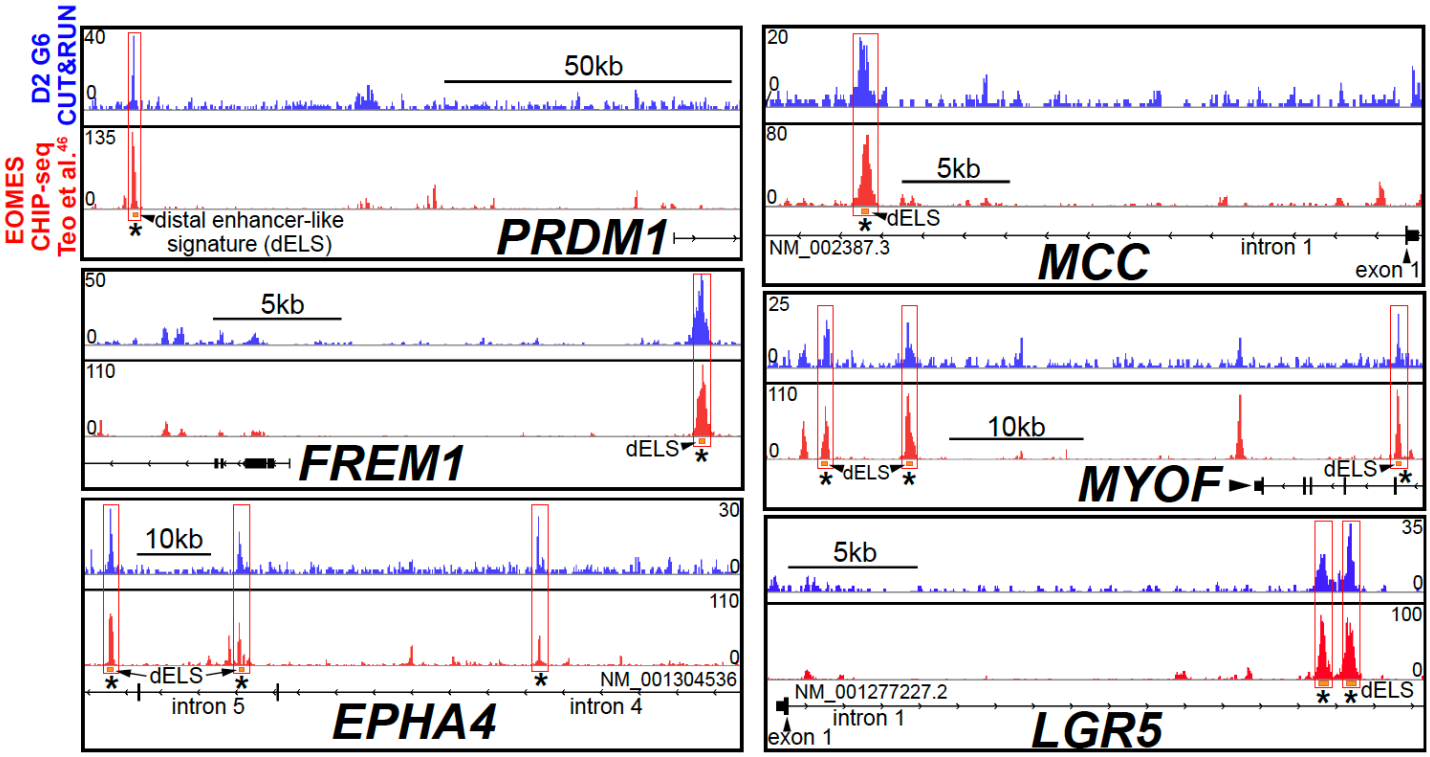

Supplemental Figure 5: GATA6 CUT&RUN peaks overlap with previously published EOMES CHIP-seq peaks. Human genome browser representations of GATA6 CUT&RUN data at day 2 of cardiac differentiation (blue tracks) and EOMES CHIP-seq identified genes at day 2 of hESC-DE differentiation from Teo et al. (Ref. 46) (red tracks). Orange rectangles represent approximate location for distal enhancer-like signatures (dELS) via the ENCODE Project (indicated by black arrows). Asterisks indicate significant GATA6 binding peaks ($p<0.003$ relative to IgG controls) and significant EOMES binding peaks as defined by Teo et al. (Ref. 46).

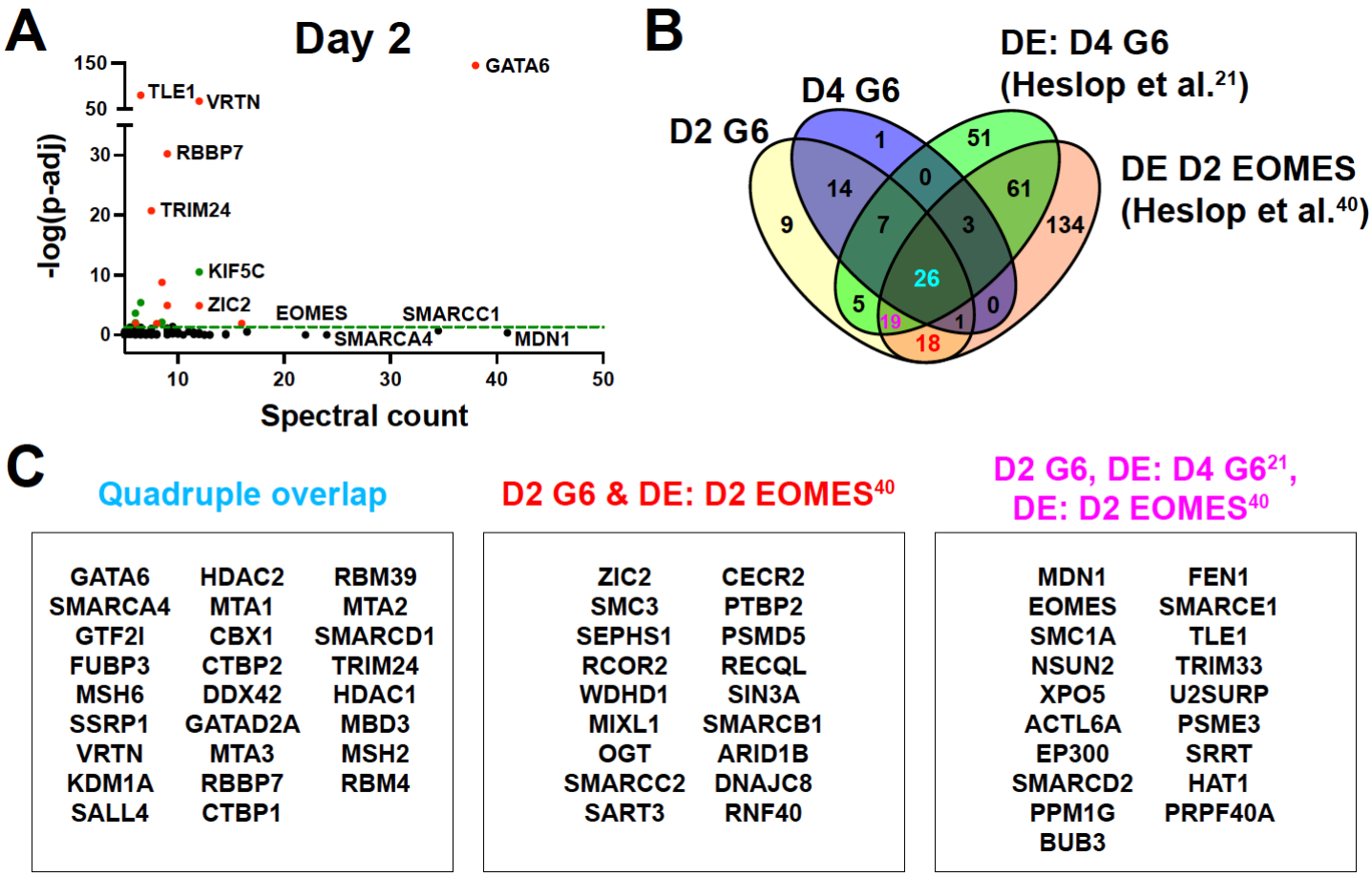

Supplemental Figure 6: Extended GATA6-RIME analysis. (**A**) Graph depicts GATA6-RIME enriched proteins (spectral count) identified at day 2 of cardiac differentiation and their corresponding day 2 RNA-seq gene expression level significance (p-adj, *GATA6*$^{-/-}$ relative to WT). Dots indicate genes, black indicates p-adj>0.05, red indicates decreased expression level (p-adj<0.05), green indicates increased expression level (p-adj<0.5). (**B**) Venn diagram comparisons for GATA6-RIME enriched proteins from day 2 (D2 G6) and day 4 (D4 G6) of cardiac differentiation from the present study with day 4 GATA6-RIME (DE: D4 G6) or day 2 EOMES-RIME (DE: D2 EOMES) enriched proteins reported during hESC-DE differentiation from Heslop et al. (Ref. 21 and Ref. 39). (**C**) Proteins identified in the Venn diagram comparisons of RIME data described in (B).

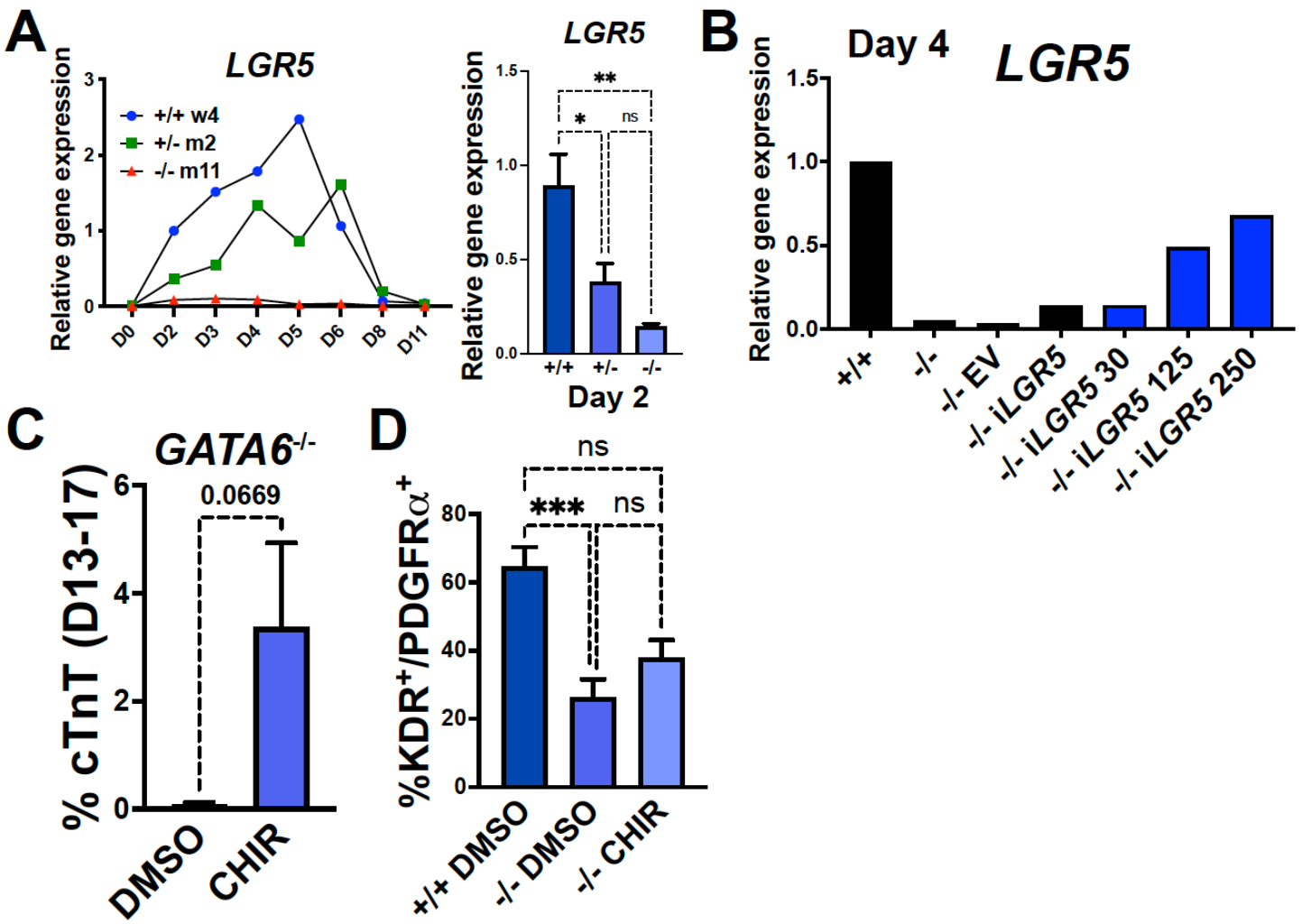

Supplemental Figure 7: Extended data for i*LGR5* and early CHIR treatment. (**A**) RT-qPCR time course for relative *LGR5* expression in differentiating *GATA6*$^{+/+}$, *GATA6*$^{+/-}$, and *GATA6*$^{-/-}$ hESCs normalized to day 2 WT gene expression level (on left). Day 2 RT-qPCR quantification for relative *LGR5* expression level normalized to WT (on right, n=6). (**B**) Day 4 RT-qPCR for relative *LGR5* expression level (normalized to WT) in i*LGR5* or EV transduced *GATA6*$^{-/-}$ hESCs treated with or without varying concentrations of DOX (30, 125, and 250 indicate ng/mL concentrations of DOX). (**C**) %cTnT^{+} CMs from days 13 to 17 of cardiac differentiation quantified by flow cytometry in *GATA6*$^{-/-}$ cells treated with CHIR (3μM) or vehicle (n≥8). (**D**) Flow cytometry quantification for %K^{+}P^{+} double-positive cells at day 5 of cardiac differentiation from *GATA6*$^{-/-}$ hESCs treated with CHIR and vehicle treated *GATA6*$^{+/+}$ or *GATA6*$^{-/-}$ hESCs controls (n≥3). Data represents the mean ± SEM, significance indicated by *p<0.05, **p<0.01, ***p<0.001, by two-tailed Student's t-test (C) or one-way ANOVA with Tukey's multiple comparisons test (A, D).

Supplemental Table 1: GATA6-RIME Enriched Proteins

99 common elements in Day_2_G6_R1 and Day_2_G6_R2		
Gene Name	**Protein Name**	**Spectral Count (Avg)**
MDN1	Midasin	41
GATA6	Transcription factor GATA-6	38
SMARCC1	SWI/SNF complex subunit SMARCC1	34.5
SMARCA4	Transcription activator BRG1	24
EOMES	Eomesodermin homolog	22
KLC3	Kinesin light chain 3	16.5
MRPL15	39S ribosomal protein L15 mitochondrial	16.5
DZIP3	E3 ubiquitin-protein ligase DZIP3	16
DNM2	Dynamin-2	14.5
GTF2I	General transcription factor II-I	14.5
FUBP3	Far upstream element-binding protein 3	13
KIF5B	Kinesin-1 heavy chain	13
MSH6	DNA mismatch repair protein Msh6	12.5
SSRP1	FACT complex subunit SSRP1	12.5
ARID1A	AT-rich interactive domain-containing protein 1A	12
GADD45GIP1	Growth arrest and DNA damage-inducible proteins-interacting protein 1	12
KIF5C	Kinesin heavy chain isoform 5C	12
VRTN	Vertnin	12
ZIC2	Zinc finger protein ZIC 2	12
KDM1A	Lysine-specific histone demethylase 1A	11.5
SALL4	Sal-like protein 4	11.5
TOP2B	DNA topoisomerase 2 (Fragment)	11.5
HDAC2	Histone deacetylase 2	11
MRPL44	39S ribosomal protein L44 mitochondrial	10.5
ELAVL1	ELAV-like protein 1	10
MTA1	Metastasis-associated protein MTA1	10
SMC1A	Structural maintenance of chromosomes protein	10
CBX1	Chromobox protein homolog 1	9.5
PYCR2	Pyrroline-5-carboxylate reductase 2	9.5
SMARCA5	SWI/SNF-related matrix-associated actin-dependent regulator of chromatin subfamily A member 5	9.5
SMC3	Structural maintenance of chromosomes protein 3	9.5
CTBP2	C-terminal-binding protein 2	9
DDX42	ATP-dependent RNA helicase DDX42	9
GATAD2A	Transcriptional repressor p66-alpha	9
MTA3	Metastasis-associated protein MTA3	9
NSUN2	tRNA (cytosine(34)-C(5))-methyltransferase	9
RBBP7	Histone-binding protein RBBP7	9
SF1	Splicing factor 1	9
SMU1	WD40 repeat-containing protein SMU1	9
XPO5	Exportin-5	9
ACTL6A	Actin-like protein 6A	8.5
SEPHS1	Selenide water dikinase 1	8.5
CTBP1	C-terminal-binding protein 1	8
EP300	Histone acetyltransferase p300	8
RBM39	RNA-binding protein 39	8
RCOR2	REST corepressor 2	8
SMARCD2	SMARCD2 protein	8
DAZAP1	DAZ-associated protein 1	7.5
HNRNPUL1	Heterogeneous nuclear ribonucleoprotein U-like protein 1	7.5
MRPL4	39S ribosomal protein L4 mitochondrial (Fragment)	7.5
MTA2	Metastasis-associated protein MTA2	7.5
SMARCD1	SWI/SNF-related matrix-associated actin-dependent regulator of chromatin subfamily D member 1	7.5
TRIM24	Transcription intermediary factor 1-alpha	7.5
WDHD1	WD repeat and HMG-box DNA-binding protein 1	7.5
HDAC1	Histone deacetylase 1	7
MIXL1	Homeobox protein MIXL1	7
OGT	UDP-N-acetylglucosamine--peptide N-acetylglucosaminyltransferase 110 kDa subunit	7
PPM1G	Protein phosphatase 1G	7
SMARCC2	SWI/SNF complex subunit SMARCC2	7
XRN2	5'-3' exoribonuclease 2	7
BUB3	Mitotic checkpoint protein BUB3 (Fragment)	6.5
DUT	DUTP pyrophosphatase isoform CRA_c	6.5
FEN1	Flap endonuclease 1	6.5
MBD3	Methyl-CpG-binding domain protein 3	6.5
MSH2	DNA mismatch repair protein Msh2	6.5
RBM4	RNA-binding protein 4	6.5
SART3	Squamous cell carcinoma antigen recognized by T-cells 3	6.5
SMARCE1	SWI/SNF-related matrix-associated actin-dependent regulator of chromatin subfamily E member 1 (Fragment)	6.5
SNX9	Sorting nexin-9	6.5
THRAP3	Thyroid hormone receptor-associated protein 3	6.5
TLE1	Transducin-like enhancer protein 1	6.5
TRIM33	E3 ubiquitin-protein ligase TRIM33 (Fragment)	6.5
U2SURP	U2 snRNP-associated SURP motif-containing protein	6.5
CECR2	Cat eye syndrome critical region protein 2	6
MRPL38	39S ribosomal protein L38 mitochondrial	6
MRPL47	39S ribosomal protein L47 mitochondrial	6
PSME3	Proteasome activator complex subunit 3	6
PTBP2	Polypyrimidine tract-binding protein 2	6
SRRT	Serrate RNA effector molecule homolog	6
USP9X	Probable ubiquitin carboxyl-terminal hydrolase FAF-X	6
DDX46	Probable ATP-dependent RNA helicase DDX46	5.5
HAT1	Histone acetyltransferase type B catalytic subunit	5.5
HINT1	Histidine triad nucleotide-binding protein 1	5.5
MRPL13	39S ribosomal protein L13 mitochondrial	5.5
MRPL20	39S ribosomal protein L20 mitochondrial	5.5
MRPL50	39S ribosomal protein L50 mitochondrial	5.5
MSI1	RNA-binding protein Musashi homolog 1	5.5
PSMD5	26S proteasome non-ATPase regulatory subunit 5	5.5
RECQL	ATP-dependent DNA helicase Q1	5.5
SIN3A	Paired amphipathic helix protein Sin3a	5.5
SMARCB1	SWI/SNF related matrix associated actin dependent regulator of chromatin subfamily b member 1 isoform CRA_c	5.5
SNRNP70	U1 small nuclear ribonucleoprotein 70 kDa	5.5
ARID1B	AT-rich interactive domain-containing protein 1B	5
DNAJC8	DnaJ homolog subfamily C member 8	5
MRPL43	39S ribosomal protein L43 mitochondrial (Fragment)	5
MRPL49	39S ribosomal protein L49 mitochondrial	5
MSI2	RNA-binding protein Musashi homolog 2	5
PRPF40A	Pre-mRNA-processing factor 40 homolog A	5
RNF40	E3 ubiquitin-protein ligase BRE1B	5
RNF40	E3 ubiquitin-protein ligase BRE1B	5

52 common elements in Day_4_G6_R1 and Day_4_G6_R2		
Gene Name	**Protein Name**	**Spectral Count (Avg)**
DNM2	Dynamin-2	24.5
GATA6	Transcription factor GATA-6	24
SMARCC1	SWI/SNF complex subunit SMARCC1	24
PYCR2	Pyrroline-5-carboxylate reductase 2	23.5
DZIP3	E3 ubiquitin-protein ligase DZIP3	21.5
SMARCA4	Transcription activator BRG1	18.5
FUBP3	Far upstream element-binding protein 3	15.5
MRPL15	39S ribosomal protein L15 mitochondrial	13
MRPL44	39S ribosomal protein L44 mitochondrial	13
SNX9	Sorting nexin-9	12
GADD45GIP1	Growth arrest and DNA damage-inducible proteins-interacting protein 1	11.5
SSRP1	FACT complex subunit SSRP1	11.5
KIF5B	Kinesin-1 heavy chain	10.5
MSH6	DNA mismatch repair protein Msh6	9.5
SALL4	Sal-like protein 4	9.5
VRTN	Vertnin	9.5
GTF2I	General transcription factor II-I	9
TRIM24	Transcription intermediary factor 1-alpha	9
ELAVL1	ELAV-like protein 1	8.5
KDM1A	Lysine-specific histone demethylase 1A	8.5
SMU1	WD40 repeat-containing protein SMU1	8.5
HDAC2	Histone deacetylase 2	8
MSI2	RNA-binding protein Musashi homolog 2	7.5
MTA1	Metastasis-associated protein MTA1	7.5
RBBP7	Histone-binding protein RBBP7	7.5
SMARCD1	SWI/SNF-related matrix-associated actin-dependent regulator of chromatin subfamily D member 1	7.5
CBX1	Chromobox protein homolog 1	7
CTBP1	C-terminal-binding protein 1	7
DDX42	ATP-dependent RNA helicase DDX42	7
KLC3	Kinesin light chain 3	7
MSH2	DNA mismatch repair protein Msh2	7
MSI1	RNA-binding protein Musashi homolog 1	7
MTA3	Metastasis-associated protein MTA3	7
SF1	Splicing factor 1	7
TAF15	TATA-binding protein-associated factor 2N	7
CTBP2	C-terminal-binding protein 2	6.5
RBM39	RNA-binding protein 39	6.5
SNRPN	Small nuclear ribonucleoprotein-associated protein N (Fragment)	6.5
TIAL1	Nucleolysin TIAR	6.5
GATAD2A	Transcriptional repressor p66-alpha	6
MRPL47	39S ribosomal protein L47 mitochondrial	6
MTA2	Metastasis-associated protein MTA2	6
RBM4	RNA-binding protein 4	6
TOP2B	DNA topoisomerase 2 (Fragment)	6
USP9X	Probable ubiquitin carboxyl-terminal hydrolase FAF-X	6
ARID1A	AT-rich interactive domain-containing protein 1A	5.5
HDAC1	Histone deacetylase 1	5.5
HNRNPUL1	Heterogeneous nuclear ribonucleoprotein U-like protein 1	5.5
MRPL4	39S ribosomal protein L4 mitochondrial (Fragment)	5.5
ADAR	Double-stranded RNA-specific adenosine deaminase	5
MBD3	Methyl-CpG-binding domain protein 3	5
MRPL49	39S ribosomal protein L49 mitochondrial	5

Supplemental Table 2: Cell lines, primer sequences, and antibodies used.

Cell Lines

Name	Source	Notes
H1-GATA6-hESCs	Parent line: WiCell Research Institute, H1 (WA01), NIHhESC-10-0043	Male
GATA6 c.1071delG iPSCs	Yu et al., 2014 (Ref: 15)	Male
293T	ATCC: human embryonic kidney cells, CRL-11268	
CF1 Mouse Embryonic Fibroblasts, irradiated	MTI Global Stem: CF-1 MEF 2M IRR	

gRNAs sequences

Name	Sequence 5' to 3'	Cell line used	Notes
G6-Cr1	GGCGTTTCTGCGCCATAAGG	H1-GATA6-hESCs	
G6-Cr2	TTATGGCGCAGAAACGCCG	H1-GATA6-hESCs	
gRNA 1 - F	caccgCACAGCCTGCAGAGCCGCGC	GATA6 c.1071delG iPSCs	gRNA target sequence capitalized
gRNA 1 - R	aaacGCGCGGCTCTGCAGGCTGTGc	GATA6 c.1071delG iPSCs	gRNA target sequence capitalized
gRNA 2 - F	caccgGTGCAGCACGGGGTCTCGAA	GATA6 c.1071delG iPSCs	gRNA target sequence capitalized
gRNA 2 - R	aaacTTCGAGACCCCGTGCTGCAc	GATA6 c.1071delG iPSCs	gRNA target sequence capitalized

Primer sequences

Name	Sequence 5' to 3'	Application
G6-iPSC-F	GCCCCTACTCGCCCTACG	PCR genotyping
G6-iPSC-R	CACCCGGACGAGAAAGTCCT	PCR genotyping
LGR5-cloning-F	TTCGTACGTACTTCGGGCACCATGGA	Full Length LGR5 PCR (using day 2 cDNA). Includes BsiWI site.
LGR5-cloning-R	GGCAATTGTTAGAGACATGGGACAAATGCC	Full Length LGR5 PCR (using day 2 cDNA). Includes MfeI site.
LGR5-seq1	GAAAGAAATGCTTTGATGGG	LGR5 Sanger sequencing primer 1
LGR5-seq2	ATGCATTTTCCACTTTGCCA	LGR5 Sanger sequencing primer 2
LGR5-seq3	CTGGTGGGAGAATGGGGTTG	LGR5 Sanger sequencing primer 3
CS-TRE-F	ATTTTCGGGTTTATTACAGG	Lentiviral vector Sanger sequencing primer
CS-TRE-R	GGAAAGGAGCTGACAGGT	Lentiviral vector Sanger sequencing primer
HPRT-F	ACCAGTCAACAGGGGACATAA	RT-qPCR
HPRT-R	CTTCGTGGGGTCCTTTTCACC	RT-qPCR
NKX2.5-F	AGCCGAAAAGAAAGAGCTGTGCG	RT-qPCR
NKX2.5-R	GACCTGCGCCTGCGAGAAGAG	RT-qPCR
TBX20-F	GGCGACGGAGAACACAATCAA	RT-qPCR
TBX20-R	CTGGGCACAGGACGACTTC	RT-qPCR
TBX5-F	AGCAGTGACTTCCTACCAGAAC	RT-qPCR
TBX5-R	TGACATTCTGTGCAGCTCCAT	RT-qPCR
GATA6-F	CTGCGGGCTCTACAGCAAG	RT-qPCR
GATA6-R	GTTGGCACAGGACAATCCAAG	RT-qPCR
GATA4-F	AAAGAGGGGATCCAAACCAG	RT-qPCR
GATA4-R	TTGCTGGAGTTGCTGGAAG	RT-qPCR
MEF2C-F	CTGGTGTAACACATCGACCTC	RT-qPCR
MEF2C-R	GATTGCCATACCCGTTCCCT	RT-qPCR
ALDH1A2-F	GGAGTCCCTTTGACCCCACCACT	RT-qPCR
ALDH1A2-R	CCCTTTCGGCCCAGTCCTTTGC	RT-qPCR
LGR5-F	GTTTCCCGCAAGACGTAACT	RT-qPCR
LGR5-R	CAGCGTCTTCACCTCCTACC	RT-qPCR
T-F	ACCCAGTTCATAGCGGTGAC	RT-qPCR
T-R	CCATTGGGAGTACCCAGGTT	RT-qPCR
EOMES-F	CTGCCCACTACAATGTGTTCG	RT-qPCR
EOMES-R	GCGCCTTTGTTATTGGTGAGTTT	RT-qPCR

Antibodies

Antibody	Source	Application
mouse monoclonal α-Actinin	Sigma-Aldrich A7811	immunocytochemistry 1:200
rabbit polyclonal NANOG	Cell Signaling Technology 3850	immunocytochemistry 1:250
rabbit polyclonal SOX2	Invitrogen 48-1400	immunocytochemistry 1:100
mouse monoclonal cardiac troponin T	Invitrogen MA5-12960	immunocytochemistry 1:200, flow cytometry 1:500
rabbit monoclonal GATA6	Cell Signaling Technology 5851	western blotting 1:1000
mouse monoclonal β-actin	Sigma-Aldrich A1978	western blotting 1:50000
mouse monoclonal anti-human KDR PE conjugated	R&D Systems FAB357P-100	flow cytometry 10μL per million cells
mouse monoclonal anti-human PDGFRα PE conjugated	R&D Systems FAB1264A	flow cytometry 10μL per million cells
goat polyclonal anti-human/mouse Brachyury PE-conjugated	R&D Systems IC2085P	flow cytometry 1:40
rabbit polyclonal SMAD2/3	Cell Signaling Technology 3102	western blotting 1:500
rabbit monoclonal Phospho-SMAD2 (Ser465/467)/SMAD3 (Ser423/425) (D27F4)	Cell Signaling Technology 8828	western blotting 1:500
rabbit monoclonal Phospho-SMAD1 (Ser463/465)/ SMAD5 (Ser463/465)/ SMAD9 (Ser465/467) (D5B10)	Cell Signaling Technology 13820	western blotting 1:500
rabbit monoclonal non-phospho (Active) β-Catenin (Ser33/37/Thr41) (D13A1)	Cell Signaling Technology 8814	western blotting 1:1000
rabbit polyclonal β-Catenin	Cell Signaling Technology 9562	western blotting 1:1000
rabbit monoclonal SMARCC1/BAF155 (D7F8S)	Cell Signaling Technology 11956	western blotting 1:1000
rabbit polyclonal TBR2 / Eomes	Abcam ab23345	western blotting 1:500
goat anti-mouse IgG1 Alexa Fluor™ 488	Invitrogen A-21121	immunocytochemistry 1:500
goat anti-rabbit Alexa Fluor™ 488	Invitrogen A-11008	immunocytochemistry 1:1000
goat anti-mouse Alexa Fluor™ 488	Invitrogen A-10667	immunocytochemistry 1:500
goat anti-mouse Alexa Fluor™ 647	Invitrogen A-21236	flow cytometry 1:400
goat anti-rabbit HRP	Bio-Rad 1706515	western blotting 1:2000 - 1:10000
goat anti-mouse HRP	Bio-Rad 1706516	western blotting 1:2000 - 1:10000
mouse monoclonal IgG1 APC-conjugated	R&D Systems IC002A	flow cytometry 10μL per million cells
mouse monoclonal IgG1 PE-conjugated	R&D Systems IC002P	flow cytometry 10μL per million cells
goat polyclonal IgG PE-conjugated	R&D Systems IC108P	flow cytometry 1:40